MORPHOLOGY OF 15 SOUTHERN EARLY-TYPE DISK GALAXIES

Eija Laurikainen and Heikki Salo

Division of Astronomy, Department of Physical Sciences, University of Oulu, Oulu, Finland; eija.laurikainen@oulu.fi

Ronald Buta

Department of Physics and Astronomy, University of Alabama, Tuscaloosa, AL, USA

Johan Knapen

Centre for Astrophysics Research, University of Hertfordshire, Hatfield, UK

Tom Speltincx

Division of Astronomy, Department of Physical Sciences, University of Oulu, Oulu, Finland

AND

David Block

School of Computational and Applied Mathematics, University of Witwatersrand, Johannesburg, South Africa

ABSTRACT

Structural analysis has been performed for a sample of 15 southern early-type disk galaxies, mainly S0 galaxies, using high-resolution K_s-band images. The galaxies are mostly barred, and many of them show multiple structures including bars and ovals, typical for S0 galaxies. The new images are of sufficient quality to reveal new detail of the morphology of the galaxies. For example, we report a hitherto undetected nuclear ring in NGC 1387, a nuclear bar in NGC 1326, and in the residual image a weak primary bar in NGC 1317. For the galaxies we (1) measure the radial profiles of the orientation parameters derived from the elliptical isophotes, (2) apply Fourier methods for calculating tangential forces, and, in particular, (3) apply structural decomposition methods. For galaxies with multiple structures a two-dimensional method is found to be superior to a one-dimensional method but only if in addition to the bulge and the disk at least one other component is taken into account. We find strong evidence of pseudobulges in S0 galaxies: 10 of the galaxies have a shape parameter of the bulge near $n = 2$, indicating that the bulges are more disklike than following the $R^{1/4}$ law. Also, six of the galaxies have either nuclear rings, nuclear bars, or nuclear disks. In all non-elliptical galaxies in our sample the bulge-to-total (B/T) flux ratio is less than 0.4, as is typically found in galaxies having pseudobulges. In two of the galaxies the B/T flux ratio is as small as in typical Sc-type spiral galaxies. This might be the hitherto undiscovered link in the scenario in which spiral galaxies are transformed into S0 galaxies. Also, bars in S0 systems are found to be shorter and less massive and to have smaller bar torques than bars in S0/a-type galaxies.

Key words: galaxies: elliptical and lenticular, cD — galaxies: evolution — galaxies: structure

1. INTRODUCTION

Structural components of galaxies such as bars, bulges, ovals, and bar-related resonance rings are among the key factors for evaluating when present-day galaxies formed and how they have evolved over time. Bulges in early-type disk galaxies are generally assumed to be old, formed through hierarchical clustering, but they might also be more recent structures assembled by internal dynamical processes in galaxies. In favorable conditions these processes might lead to the transformation of spiral galaxies into S0 galaxies through gas stripping in the halo and the disk (Bekki et al. 2002) or due to strong and sustained star formation in the central regions of the galaxies (Kormendy & Kennicutt 2004, hereafter KK04).

In these secular evolutionary processes the relative mass of the bulge increases. In cases with gas stripping the bulges should have older stellar populations than the disks, and their surface brightness profiles are expected to resemble the $R^{1/4}$ law more than the exponential function. However, due to the small amount of gas in S0 galaxies, star formation is not expected to be the dominant mechanism for the growth of the bulge unless exceptionally strong accretion of external gas is taking place. Bulgelike mass concentrations can also form through resonant scattering or bending instabilities in the central regions of primary bars (Pfenniger

1984; Raha et al. 1991), in which case these so-called pseudobulges should have stellar populations similar to those in the underlying bars. In order to evaluate the possible role of these processes in galaxy evolution, the properties of bars, ovals, and bulges need to be systematically studied in the spiral-S0 divide, e.g., through Sa and S0/a to S0$^+$ and S0$^-$ types.

Secondary processes in galaxy evolution are generally tied to the growth of a bulge in one way or another, but an alternative approach was discussed by van den Bergh (1979, 1998), who outlined the DDO system of classification in terms of a nurture theory. In this classification system, S0 galaxies form a sequence parallel to spiral galaxies, with types S0a, S0b, and S0c being the S0 analogs of Sa, Sb, and Sc galaxies. A difficulty with this approach has been that no S0c galaxies have been found so far; that is, clear S0 galaxies showing a bulge-to-total (B/T) luminosity ratio similar to that of an Sc galaxy. However, this might be a bias due to the fact that the application of too simple analysis methods can easily hide the real nature of bulges, particularly in S0 galaxies that have rich morphological structures.

To our knowledge no previous systematic morphological study of galaxies has been carried out in the spiral-S0 divide in the near-infrared. Also, although two-dimensional (2D) decompositions have become a standard, even in recent studies (de Souza et al. 2004, hereafter SGA04; Christlein & Zabludoff 2004) multiple

TABLE 1
OBSERVATIONS

Galaxy (1)	Type (Adopted) (2)	Type (RC3) (3)	Filter (4)	FWHM (arcsec) (5)	St. Dev. (6)
ESO 208-G21[a]	E(d)5	SAB0$^-$	K_s	0.63	1.1
NGC 1079	(R$_1$R$_2'$)S$\underline{AB}$(rs)a	(R)SAB(rs)0/a	K_s	0.84	1.0
NGC 1317[b]	(R$'$)SAB(rl)a	SAB(r)a	J	0.60	1.0
			K_s	0.66	2.4
NGC 1326	(R$_1$)SAB(r)0/a	(R)SB(r)0$^+$	J	0.72	1.0
			K_s	0.72	1.0
NGC 1350	(R$'_1$)SAB(r)ab	(R$'$)SB(r)ab	K_s	0.75	1.5
NGC 1387	SB0$^-$	SAB(s)0$^-$	K_s	0.69	1.1
NGC 1411	SA(l)0°	SA(r)0$^-$	K_s	0.81	1.2
NGC 1512	(R$'$)SB(r)ab pec	SB(r)a	J	0.69	2.1
			K_s	0.63	1.0
NGC 1533	(RL)SB0°	SB0$^-$	K_s	0.66	1.3
NGC 1553	SA(rl)0$^+$	SA(rl)0°	K_s	0.75	1.2
NGC 1574[c]	SB0$\underline{^-}$	SA(s)0$^-$:	K_s	0.75	1.3
NGC 3081	(R$_1$R$_2'$)SAB(r)0/a	(R)SAB(r)0/a	J	0.69	1.5
			K_s	0.63	2.0
NGC 3100[a]	SAB(s)0$^+$ pec	SAB(s)0° pec	J	0.84	2.5
NGC 3358	(R$'_2$)SAB(l)a	(R)SAB(s)0/a	K_s	0.78	0.9
NGC 3706[a]	E$^+$4	SA(rs)0$^-$	K_s	0.81	0.8

NOTE.—If not otherwise mentioned, the classifications in col. (2) are from BCO06.
[a] The classification in col. (2) is made by R. Buta, based on our K_s-band image.
[b] For this galaxy the residual image shows a weak classical bar.
[c] The residual image for this galaxy shows a complete inner ring of r-variety.

structures have not been taken into account. The current study is the third paper in a series in which the morphological properties of a sample of 170 early-type disk galaxies are studied. The description of the sample and the first results are presented in Laurikainen et al. (2005, hereafter Paper I) and in Buta et al. (2006b, hereafter Paper II). In Paper I we found, for a subsample of 24 S0–S0/a galaxies, that the B/T flux ratios are significantly smaller and the bulges more disklike than is generally assumed for their morphological type. In Paper II we investigated in detail the Fourier properties of early-type bars and ovals. We found that they can be well described in terms of single- or double-Gaussian components of the relative Fourier amplitudes of density. In this study we analyze the morphological properties of 15 southern galaxies of the de Vaucouleurs revised Hubble types S0$^-$ to Sa, mainly S0 galaxies, with a large range of apparent bar strengths. For these galaxies we use K_s-band images to derive the orientation parameters from the elliptical isophotes, apply Fourier methods for calculating non-axisymmetric forces, and perform 2D multicomponent structural decompositions. The multicomponent decompositions are compared with more simple bulge-disk decompositions and with one-dimensional (1D) decompositions for the same galaxies.

2. SAMPLE AND DATA REDUCTIONS

We use a subsample of 15 galaxies of the Near-Infrared S0 Survey (NIRS0S), which was originally drawn from the Third Reference Catalog of Bright Galaxies (RC3; de Vaucouleurs et al. 1991) using the following selection criteria: $-3 \leq T < 2$, $B_T < 12.5$ mag, and $\log R_{25} < 0.35$, yielding a sample of 170 galaxies. The final sample consists of 190 galaxies, because 20 late-type elliptical galaxies classified as S0 by Sandage were also added. This is to take into account the misclassified elliptical galaxies in RC3. The original sample was selected to be similar in size to the Ohio State University Bright Galaxy Survey (OSUBGS; Eskridge et al. 2002) for spiral galaxies. The properties of the sample are described in more detail in Paper II.

The observations were carried out in 2004 December using the SOFI instrument, attached to the 3.5 m New Technology Telescope at ESO. High-resolution K_s-band images (0″29 pixel^{-1}) were obtained for all galaxies, and for five of them J-band images were also obtained. The total on-source integration time was 1800–2400 s in the K_s band and 1200 s in the J band, mostly taken in snapshots of 3–6 s. Owing to the high sky brightness in the near-infrared, the sky fields were taken alternating between the galaxy and the sky field in time intervals of 1 minute; in the object a random dithering within a box of 20″ was used, whereas the sky fields were randomly selected, carefully avoiding bright foreground stars. The observations were obtained in good atmospheric conditions, the nights being mainly photometric. The mean stellar full width at half-maximum (FWHM) is 0″72 in the K_s band. The sample and the seeing conditions are shown in Table 1, where "St. Dev." is the standard deviation of the mean in the sky background. The galaxy classifications in column (3) are from RC3. The adopted morphological type in column (2) is mainly from Buta et al. (2006a, hereafter BCO06), or the classification is judged by R. Buta using the images in the Sandage & Bedke (1994) catalog. For NGC 3706 and ESO 208-G21, the classification is based on the K_s-band images from this study.

The images were processed using IRAF[1] package routines. The reduction steps consisted of sky subtraction, flat-fielding of the individual difference images, removal of foreground stars, and transposing the images to have north up and west on the right. Dome flats were used, in which shade patterns due to the scattered light were corrected. The uneven illumination of the screen was also corrected in the flat fields using a correction frame created from multiple observations of one standard star. The standard star observation was used to create a surface that was then normalized

---

[1] IRAF is distributed by the National Optical Astronomy Observatory, which is operated by the Association of Universities for Research in Astronomy, Inc., under cooperative agreement with the National Science Foundation.
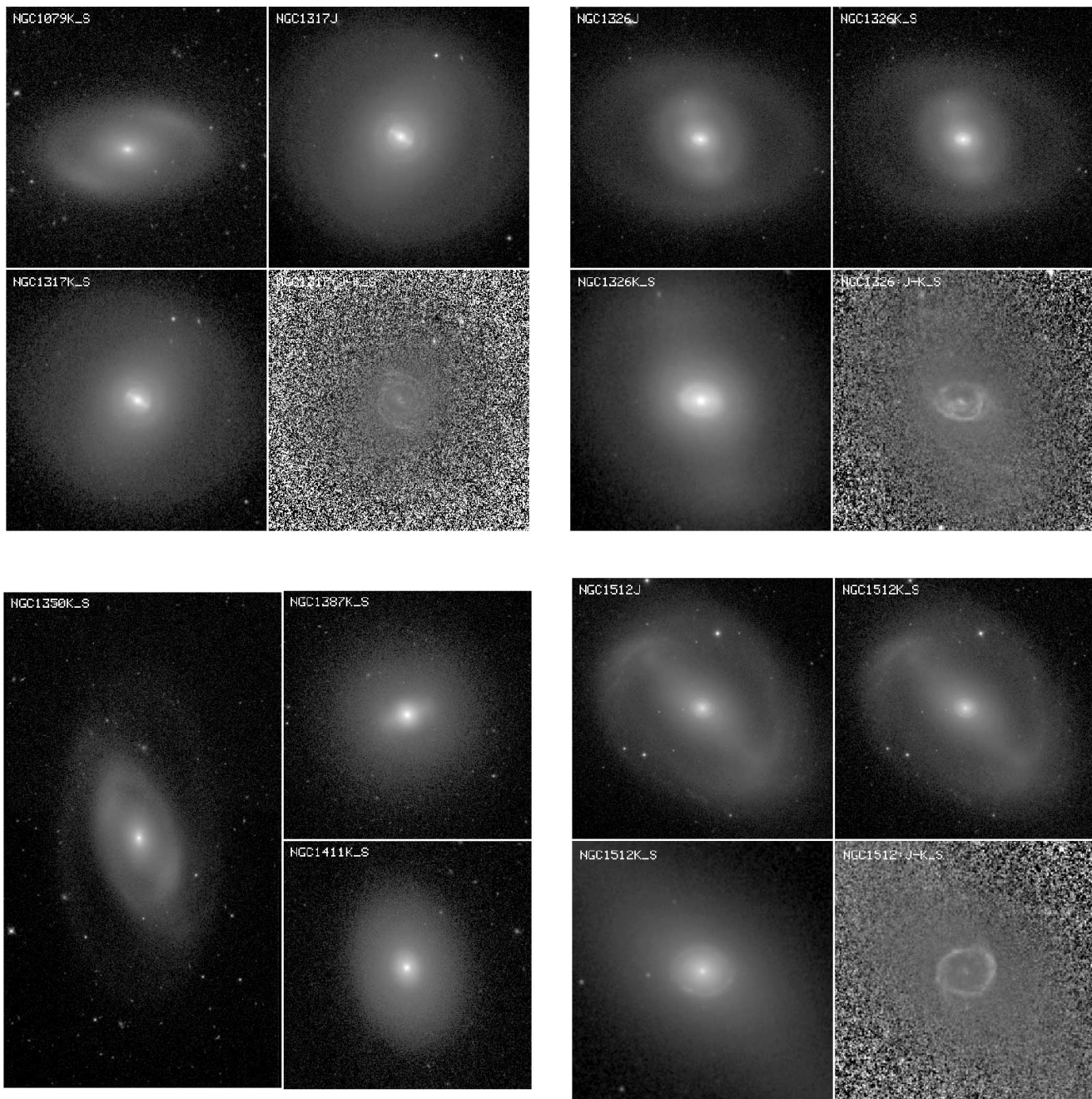
Fig. 1.—Direct K_s-band images and $J - K_s$ color index maps for the sample galaxies. The color index maps are coded so that redder features are lighter. The images are shown in the plane of the sky so that north is up and east is left. Note that for galaxies NGC 1326, NGC 1512, NGC 1553, NGC 3081, NGC 3100, and NGC 3358 the inner regions of the galaxies are also shown.

to unity. For these corrections IRAF scripts offered by ESO were used. The images were cleaned of foreground stars by finding the stars with DAOFIND and then using a stellar point-spread function (PSF) to remove the stars. Any residuals left by the PSF fitting were cleaned using the IRAF routine *imedit*. For five of the galaxies $J - K_s$ color maps were also constructed. The images and the color maps are shown in Figure 1. All direct images in Figure 1 are in units of mag arcsec^{-2} and are generally displayed from $\mu_{K_s} = 12.0$ to 22.0 mag arcsec^{-2}. Color index maps display colors in the range $0.5 < J - K_s < 1.5$.

3. ELLIPTICAL ISOPHOTES

The elliptical isophotes were derived mainly in the K_s band using the *ellipse* routine in IRAF. We calculate the radial profiles

of the position angles ϕ and the ellipticity $\epsilon = 1 - q$, where q is the minor-to-major axis ratio (see Fig. 2). The profiles were calculated both in linear and in logarithmic scale: the linear scale for deriving the orientation parameters of the outer disks and the logarithmic scale for identifying the structural components, particularly in the inner regions of the galaxies. The isophotal fits were made to the original images. When available, J-band images were used to estimate the orientation parameters, because they were generally deeper than the K_s-band images. In the isophotal fitting deviant pixels above $3\,\sigma$ were rejected. The parameters ϕ and q are listed in Table 2, calculated as mean values in the radial range indicated in the table. The uncertainties are standard deviations of the mean in the same radial range. Also shown are the orientation parameters given in RC3, and for some of the galaxies
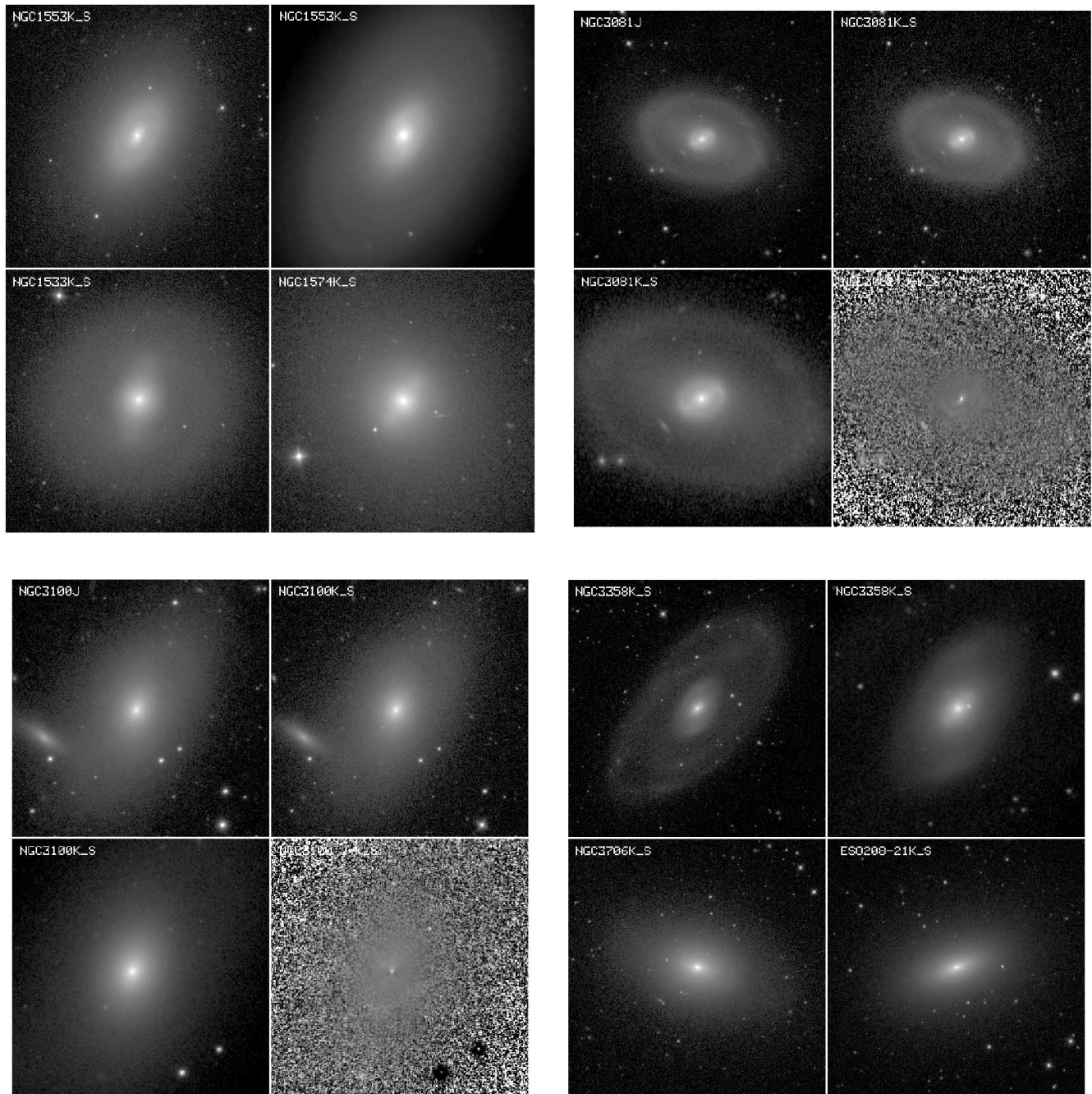
Fig. 1.—*Continued*

values from other sources are shown as well. The values used in this study are marked with an asterisk. In the analysis orientation parameters derived in this study are used, except for galaxies NGC 3081, NGC 1512, and NGC 1326. For the first two galaxies we use kinematical estimates of ϕ obtained by Buta & Purcell (1998) and Buta (1988), respectively, and for NGC 1326 the photometric estimates by Buta (1988) are used.

A comparison with RC3 shows large deviations in the orientation parameters, in particular for the galaxies NGC 1079 (ϕ), NGC 1317 (q and ϕ), NGC 1512 (ϕ), NGC 1533 (q and ϕ), and NGC 3081 (q and ϕ). However, our measurements are generally in good agreement with those measurements given in the literature where deep optical or infrared images are used. This is the case for NGC 1512, for which Kuchinski et al. (2000) obtained $\phi = 56°$. For NGC 3081 Buta & Purcell (1998) give photomet-

rically estimated values of $\phi = 86°$ and $q = 0.837$. Also, for NGC 1350 our measurements for the orientation parameters are in agreement with those obtained by Garcia-Gomez et al. (2004).

4. FOURIER DECOMPOSITIONS

For estimating tangential forces induced by nonaxisymmetric structures in galaxies we use a gravitational bar torque approach (Combes & Sanders 1981; Quillen et al. 1994), first applied to galaxy samples by Buta & Block (2001) and Laurikainen & Salo (2002). The polar method we use has been described by Laurikainen & Salo (2002), Salo et al. (2004), and Laurikainen et al. (2004a, hereafter LSB04: see also Salo et al. 1999). The gravitational potential is inferred from the 2D K_s-band image by assuming that the near-infrared light distribution traces the mass and that the mass-to-luminosity flux ratio is constant. It is assumed
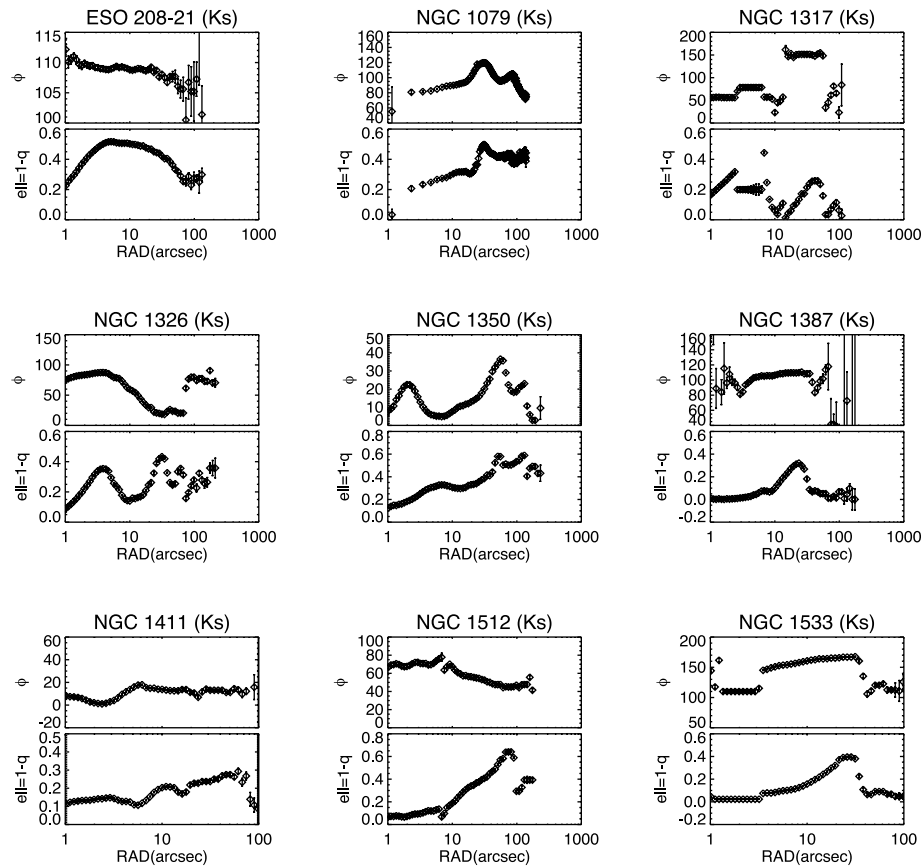
Fɪɢ. 2.—Radial profiles of the position angles ϕ and ellipticities $\epsilon = 1 - q$, where q is the minor to major axis ratio, derived using the *ellipse* routine in IRAF.

that the vertical profile is exponential and that the vertical scale height depends on the morphological type. Deprojected images were used, which were constructed by first subtracting off the bulge model, deprojecting only the disk light, and then adding back the bulge as an assumed spherical component (see § 5 for more sophisticated decompositions). The derived gravitational potentials are used to calculate maps of the maximum ratio of the tangential force (F_T) to the azimuthally averaged radial force (F_R), as well as a radial profile of the maximum relative tangential force at each distance (see Fig. 3),

$$Q_T(r) = \frac{|F_T(r, \phi)|_{max}}{\langle|F_R(r, \phi)|\rangle}, \qquad (1)$$

where $\langle|F_R(r, \phi)|\rangle$ denotes the azimuthally averaged axisymmetric force for each r-value. The maximum value of this profile, Q_g at a radius r_{Qg}, gives a single measure of *bar strength* for these early-type galaxies, for which spiral arm torques are generally negligible. In the calculation of the gravitational potential we use azimuthal Fourier decompositions in radial annulae, typically using even components with azimuthal wavenumber $m < 20$. The gravitational potential is then calculated using a fast Fourier transform in the integration over azimuth and direct summation in radial coordinates. An important advantage of this method compared to the more straightforward Cartesian integration ("Quillen's method") is the suppression of spurious force maxima in the outer disk arising due to noise. The other advantage is that it simultaneously gives the relative mass of the bar, as estimated from the maxima of $m = 2$ and 4 amplitudes of density (A_2 and A_4, respectively). The measurements are shown in Table 3, where the bar lengths are also given. Bar length is

identified within the region in which the phase of the $m = 2$ amplitude is maintained nearly constant. If no bar length is given, the parameters indicate the properties induced by other nonaxisymmetric components such as ovals or inner disks. The errors are formal errors related to Q_g measurements in the four image quadrants. It is worth noting that a peak in a Q_T-profile should not be automatically interpreted as indicating the presence of a bar. For example, in NGC 3100 strong tangential forces are detected at $r < 40''$, although there is no bar in this galaxy. As discussed in § 5, this galaxy is dominated by a large oval, which appears as a nonaxisymmetric structure in the Fourier analysis. Because of the high uncertainty in the position angle of NGC 1512, no Q_g value for this galaxy is given in Table 3: the kinematic estimate by Buta (1988) gives $\phi = 83°$, while we measure $\phi = 46°$.

5. STRUCTURAL DECOMPOSITIONS

5.1. *The Algorithm*

We use a 2D multicomponent decomposition code, originally presented in Paper I (see also LSB04), where the code was also tested. In this study we also use a 1D version of the code (Laurikainen & Salo 2000), which can be efficiently used in conjunction with the 2D code.

In the 2D multicomponent code all components use generalized elliptical isophotes (Athanassoula et al. 1990), the isophotal radius being described by the function

$$r = (|x|^{c+2} + |y/q|^{c+2})^{1/(c+2)}. \qquad (2)$$

The isophote is boxy when the shape parameter $c > 0$, disky when $c < 0$, and purely elliptical when $c = 0$. Circular isophotes correspond to $c = 0$ and minor-to-major axial ratio $q = 1$.
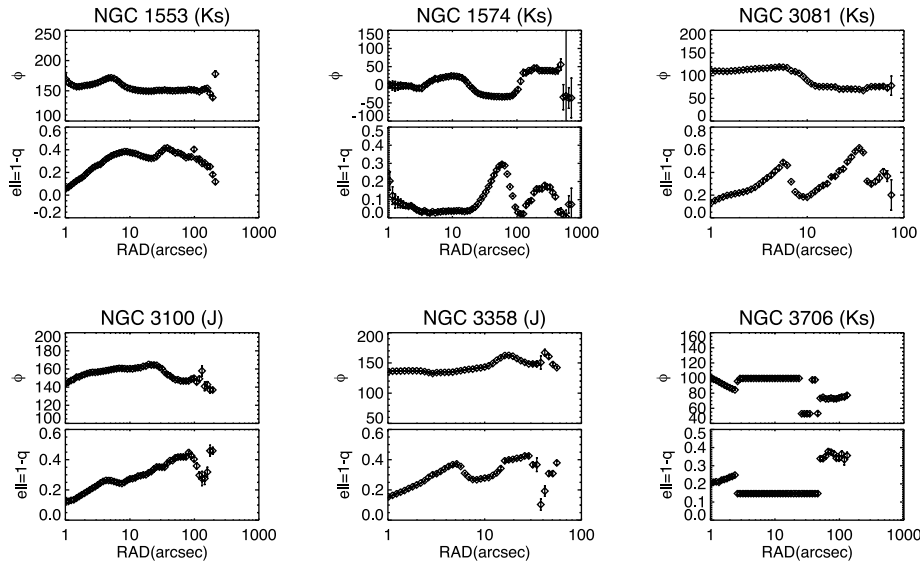
Fig. 2.—*Continued*

The disks are described by an exponential function,

$$I_d(r_d) = I_{0d} \exp\left[-(r_d/h_r)\right], \qquad (3)$$

where I_{0d} is the central surface density of the disk and h_r is the radial scale length of the disk. The radius r_d is calculated along the disk plane defined by the assumed ϕ- and q-values (for disk $c = 0$). The surface brightness profiles of the bulges are described by a generalized Sérsic function,

$$I_b(r_b) = I_{0b} \exp\left[-(r_b/h_b)^\beta\right], \qquad (4)$$

where I_{0b} is the central surface density, h_b is the scale parameter of the bulge, and $\beta = 1/n$ determines the slope of the pro-

jected surface brightness distribution of the bulge ($n = 1$ for exponential and $n = 4$ for the $R^{1/4}$ law). The parameter r_b is the isophotal radius defined via the parameters q_b, c_b, and ϕ_b, where the subscript stands for the bulge. In the case of an elliptical bulge, ϕ_b is its major-axis position angle measured counterclockwise from north in the sky plane. The Sérsic function can also be applied for the other nonaxisymmetric components, or, alternatively, the Ferrers function can be used, described as

$$I_{\text{bar}}(r_{\text{bar}}) = \begin{cases} I_{0\text{bar}}\left[1 - (r_{\text{bar}}/a_{\text{bar}})^2\right]^{n_{\text{bar}}+0.5}, & r_{\text{bar}} < a_{\text{bar}}, \\ 0, & r_{\text{bar}} > a_{\text{bar}}, \end{cases} \qquad (5)$$

TABLE 2
ORIENTATION PARAMETERS

Galaxy	Filter	ϕ (Measured) (deg)	q (Measured)	Range (arcsec)	ϕ (RC3) (deg)	q (RC3)	ϕ/q (Other)
ESO 208-G21	K_s	109 ± 1*	0.722 ± 0.024*	93–116	110	0.708	108/0.70[a]
NGC 1079..................	K_s	78 ± 2*	0.590 ± 0.011*	116–128	87	0.607	...
NGC 1317..................	J	91 ± 2*	0.953 ± 0.004*	75–87	78	0.871	...
NGC 1326..................	J	75.6 ± 1.1	0.729 ± 0.000	134–140	77	0.741	73.4/0.750*[b]
NGC 1350..................	K_s	6 ± 1*	0.586 ± 0.004*	120–125	0	0.540	6/0.51[c]
NGC 1387..................	K_s	128 ± 10*	0.998 ± 0.069*	65–70	...	0.000	131/0.98[d]
NGC 1411..................	K_s	9 ± 0*	0.729 ± 0.002*	70–74	6	0.724	...
NGC 1512..................	J	46 ± 0	0.605 ± 0.009*	140–146	90	0.631	56/0.64[e], 83*[f]
NGC 1533..................	K_s	116 ± 5*	0.942 ± 0.006*	55–70	151	0.851	...
NGC 1553..................	K_s	150 ± 6*	0.749 ± 0.000*	130–180	150	0.633	.../0.93 [d]
NGC 1574..................	K_s	31 ± 1*	0.960 ± 0.003*	95–100	35	0.000	...
NGC 3081..................	J	110 ± 10	0.861 ± 0.018*	72–88	158	0.776	97/0.837*[g]
NGC 3100..................	J	148 ± 1*	0.603 ± 0.012*	105–115	154	0.513	...
NGC 3358..................	K_s	138 ± 0*	0.581 ± 0.012*	64–70	141	0.562	125/0.74[h]
NGC 3706..................	K_s	76 ± 1*	0.634 ± 0.011*	122–140	78	0.603	...

NOTE.—Asterisks denote values used in this study.
[a] Martel et al. (2004), their Fig. 2.
[b] Buta et al. (1998).
[c] Garcia-Gomez et al. (2004).
[d] NASA/IPAC Extragalactic Database.
[e] Kuchinski et al. (2000).
[f] Buta (1988).
[g] Buta & Purcell (1998); ϕ is kinematic, and q is photometric.
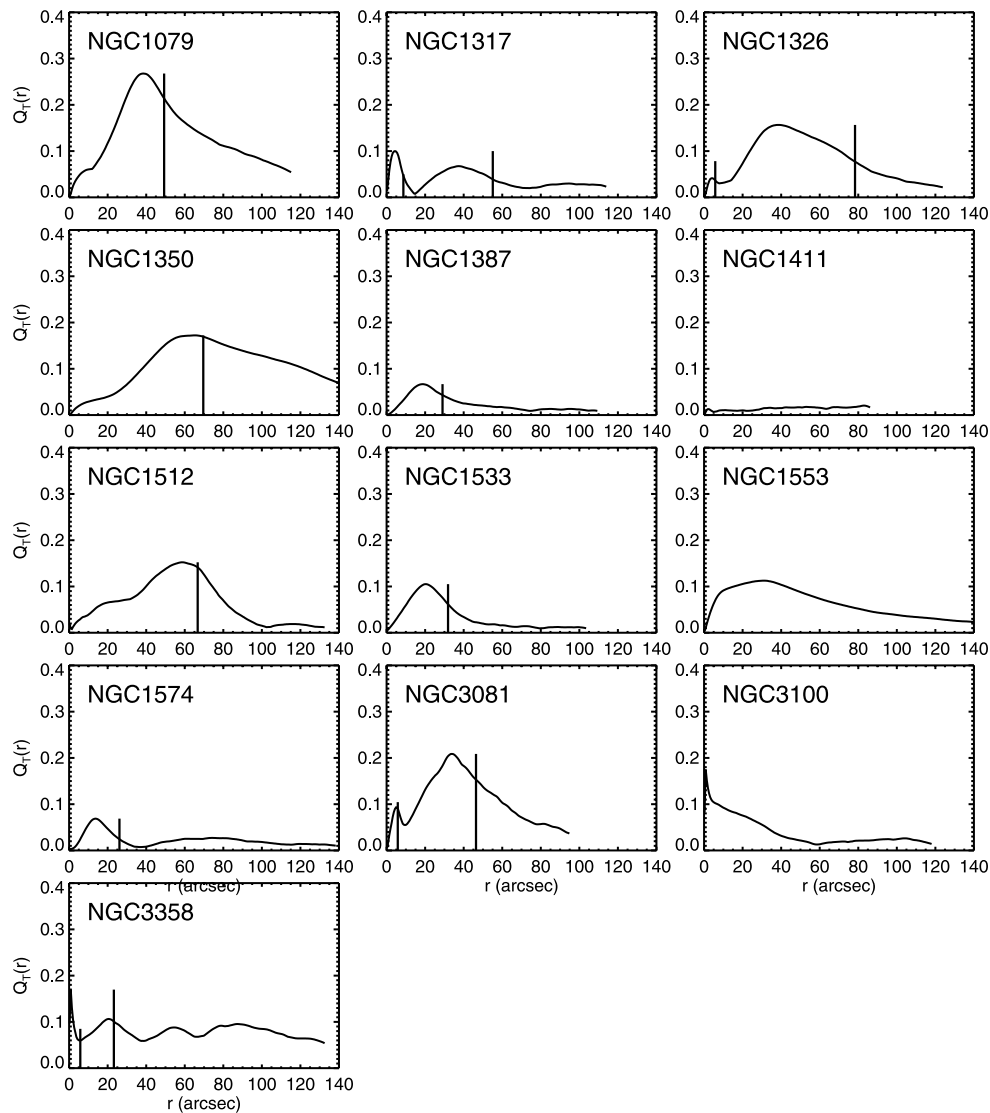[h] Erwin (2004).

FIG. 3.—Radial profiles $Q_T(r)$ of the maximum relative tangential forces. The tangential force at each distance is normalized to the azimuthally averaged radial force at that distance (see the text for more detail). The lengths of the primary and secondary bars are indicated by thick vertical lines. Note that not all Q_T maxima are induced by bars.

where I_{0bar} is the central surface brightness of the bar, a_{bar} is the bar major axis length, and n_{bar} is the exponent of the bar model defining the shape of the bar radial profile. The isophotal radius (r_{bar}) is defined via the parameters q_{bar}, c_{bar}, and ϕ_{bar}. As in the 2D version, in the 1D version the bulges are described by a Sérsic function.

5.2. The Fitting Procedure

The fitting was made in flux units in the plane of the sky. Depending on the choice of the weighting function, more weight can be assigned to the pixels in the central parts of the galaxies, where the flux level is high, or to the outer regions, where the number of pixels is high. In this study we generally use $w_i = 1/F$, where F is the model flux in pixel i. However, it was shown in Paper I that our method is not sensitive to the choice of the weighting function. In order to account for the effects of seeing, the model is convolved with a Gaussian PSF using a FWHM measured for each image.

Due to the large number of free parameters in the 2D approach, the fitting is time consuming. In order to speed the process a good fit was found first using the images rebinned by a factor of 4; these

results were then used as initial parameters for more sophisticated decompositions performed for the original images. Generally, the decompositions were started by finding h_r. In cases in which the presence of an extended disk was not immediately obvious, spiral arms or rings were used to confirm the presence of the underlying disk. In some cases they were visible only after subtracting the bulge or disk model. A few images were too noisy for finding h_r in a reliable manner with the 2D code, in which case the 1D code was used by fitting an exponential to the outer parts of the disk.

Three different kinds of 2D decompositions were made: (1) multicomponent ($N_{max} = 5$), (2) three-component (typically bulge-disk-bar), and (3) two-component (bulge-disk) decompositions. In addition, simple three-component decompositions were made by assuming that the bulges have spherical light distributions. Such decompositions are required for deprojecting the images, because it is difficult to make a 3D bulge model allowing for flattening or triaxiality for the bulge. As not all bulges are spherical, some caution is needed while interpreting the innermost structures of the deprojected images. The best-fitting multicomponent decompositions are compiled in Table 4 and illustrated in Figure 4. Component 1 is in most cases the primary bar, but in

TABLE 3
RESULTS OF THE FOURIER ANALYSIS

Galaxy	Bar Length (arcsec)	Q_g	r_{Qg} (arcsec)	A_2	A_4
		Southern Sample			
NGC 1079..............	49.3	0.268 ± 0.047	38.6	0.80	0.32
NGC 1317..............	55.1	0.065 ± 0.005	40.0	0.30	0.08
NGC 1317..............	8.7	0.100 ± 0.002	4.3	0.38	0.20
NGC 1326..............	78.3	0.157 ± 0.006	38.6	0.67	0.24
NGC 1326..............	5.8	0.040 ± 0.005	4.4	0.24	0.03
NGC 1350..............	69.6	0.172 ± 0.044	65.3	0.63	0.21
NGC 1387..............	29.0	0.067 ± 0.004	18.9	0.39	0.15
NGC 1533..............	31.9	0.105 ± 0.008	20.6	0.42	0.19
NGC 1553..............	. . .	0.113 ± 0.001	31.0	0.35	0.06
NGC 1574..............	26.1	0.069 ± 0.006	13.6	0.34	0.15
NGC 3081..............	46.4	0.209 ± 0.005	34.0	0.85	0.34
NGC 3081..............	5.8	0.100 ± 0.002	4.5	0.40	0.11
NGC 3100..............	. . .	0.100 ± 0.006	6.0	0.21	. . .
NGC 3358..............	23.2	0.100 ± 0.000	20.3	0.40	0.15
NGC 3358..............	5.8	0.170 ± 0.000	3.0	0.20	. . .
		Northern Sample			
NGC 718................	32.2	0.121 ± 0.011	18.2	0.41	0.20
NGC 718................	13.8	0.030 ± 0.000	1.1	0.15	. . .
NGC 936................	59.8	0.202 ± 0.036	37.0	0.58	0.30
NGC 1022..............	27.6	0.143 ± 0.009	15.9	0.41	0.14
NGC 1400..............	. . .	0.034 ± 0.001	. . .	0.11	. . .
NGC 1415..............	71.3	0.240 ± 0.046	47.2	0.80	0.25
NGC 1440..............	27.6	0.141 ± 0.004	17.7	0.50	0.23
NGC 1452..............	46.0	0.420 ± 0.044	36.1	0.90	0.58
NGC 2196..............	. . .	0.067 ± 0.018	. . .	0.15	. . .
NGC 2273..............	41.4	0.201 ± 0.013	20.0	0.57	0.25
NGC 2460..............	9.2	0.077 ± 0.028	4.4	0.14	0.04
NGC 2681..............	27.6	0.040 ± 0.000	16.1	0.23	0.06
NGC 2681..............	4.6	0.010 ± 0.000	2.3	0.10	0.03
NGC 2681..............	64.4	0.059 ± 0.001	54.5	0.30	0.07
NGC 2781..............	62.1	0.067 ± 0.000	34.5	0.46	0.10
NGC 2855..............	. . .	0.075 ± 0.009	. . .	0.15	. . .
NGC 2859..............	69.0	0.101 ± 0.003	41.6	0.57	0.22
NGC 2859..............	6.9	0.030 ± 0.000	3.5	0.15	0.03
NGC 2911..............	. . .	0.081 ± 0.011	. . .	0.20	. . .
NGC 2983..............	41.4	0.299 ± 0.027	24.6	0.77	0.45
NGC 3626..............	39.1	0.109 ± 0.003	20.5	0.35	0.08
NGC 3941..............	29.9	0.086 ± 0.002	20.0	0.34	0.14
NGC 4245..............	50.6	0.185 ± 0.007	29.2	0.54	0.20
NGC 4340..............	78.2	0.241 ± 0.016	55.9	0.55	0.27
NGC 4340..............	4.6	0.020 ± 0.000	5.8	0.05	. . .
NGC 4596..............	78.2	0.276 ± 0.050	48.5	0.67	0.36
NGC 4608..............	57.5	0.251 ± 0.011	37.5	0.77	0.47
NGC 4643..............	57.5	0.299 ± 0.007	40.7	0.85	0.55

nonbarred galaxies it can be an oval or an inner disk. Component 2 generally refers to the secondary bar or oval and component 3 to a large tertiary bar or oval. The B/T flux ratio can be calculated either using the disk-component extrapolated to infinity or by limiting to the fitted region alone: in this study the nonextrapolated disk is used.

To be sure that we were fitting real structures, a preliminary identification of bars, ovals, and disks was made by inspecting (1) the original images and the $J - K$ color maps, (2) the radial profiles of the orientation parameters, and (3) the profiles of the Fourier amplitudes of density. In addition, in some cases the bulge or disk-model-subtracted images were inspected afterward. The nonaxisymmetric structures appear as bumps in the ϵ-profiles,

provided that their surface brightnesses are high enough compared to that of the underlying disk. Also, the position angles show isophotal twists in the bar regions. The even Fourier amplitudes of density are particularly sensitive for detecting the nonaxisymmetric structures in galaxies. The identifications of the morphological components and the ring dimensions are shown in Tables 5 and 6. As in Table 4, in Table 5 the subscripts 1 and 2 refer to the primary and secondary bars/ovals. Following KK04 we adopt the terminology that the flat inner structure is called a "lens" if the morphological type is S0–S0/a and an "oval" when the galaxy has a later morphological type. A lens was originally defined by Kormendy (1979) as a feature showing a shallow brightness gradient interior to a sharp edge, whereas an oval was defined as having a broad elongation in the light distribution. It seems that in some cases the division according to the morphological type is artificial. S0 galaxies can actually have both ovals and lenses. However, as the discrimination between ovals and lenses is not straightforward, we keep the present terminology.

5.3. Discussion of Individual Galaxies

In the following we discuss the morphological properties of the individual galaxies, which in early-type disk galaxies are generally rich. Detecting these structures depends not only on the wavelength but also on the image resolution and the integration time used. We use deep, high-resolution near-infrared images, but in spite of that it is sometimes difficult to identify the structural components, particularly the bulges. In order to illustrate this, some details of the decompositions are also given. In most cases it was not possible to use any semiautomatic procedure to find reliable solutions.

ESO 208-G21: ESO 208-G21 is a bulge-dominated system with an elongated inner structure. Most likely for this reason Corwin et al. (1985, p. 185) classified it as E4, whereas in RC3 the inner structure was interpreted to be a weak bar/oval, leading to a classification of SAB0$^-$. Martel et al. (2004) found that the inner structure is a dusty inner disk, based on the analysis of high-resolution *Hubble Space Telescope* (*HST*) images. The disk is clearly visible in our unsharp-masked image (Fig. 5), and it can also be identified in the ellipticity profile as a peak, followed by a decline up to the radius at which the dominance of the bulge makes the profile flat. The ellipticity profile we find is very similar to that obtained previously by Scorza et al. (1998), who also made a structural decomposition for this galaxy. As they use a different method than we do, it is interesting to compare the results: in both cases a solution was found in which the galaxy has a small exponential inner disk embedded in a large massive bulge. The $B/T = 0.97$ we found is very similar to the $B/T = 0.92$ obtained by Scorza et al. in the V band (they give $D/B = 0.09$). The decomposition by Scorza et al. is based on an iterative process in which the disk is first subtracted and the isophotes of the remaining bulge component are inspected. The procedure is repeated until perfect elliptical isophotes remain. It is worth noting that for this galaxy our 1D and 2D codes give very similar solutions. Obviously, this galaxy has no outer disk, and the bulge is strongly flattened. We classify this galaxy as E(d)5, thus confirming the earlier classification by Kormendy & Bender (1996).

NGC 1079: The morphology of NGC 1079 has been previously studied by Buta (1995), Jungwiert et al. (1997), and SGA04, who also made a 2D decomposition for it, and Knapen et al. (2006), who found a strong nuclear peak in Hα surrounded by rather faint circumnuclear patchy emission. Buta (1995) recognized NGC 1079 as a galaxy showing one of the largest examples of a feature called R_1R_2', a double outer ring/pseudoring morphology

TABLE 4
Decomposition Results

		Bulge				Disk	Component 1		Component 2		Component 3		
Galaxy	n	r_{eff} (arcsec)	q	fii_1 (deg)	fii_2 (deg)	h_R (arcsec)	q	fii (deg)	q	fii (deg)	q	fii (deg)	B/T
ESO 208-G21	4.2	11.60	0.60	0	...	1.4[a]	...	...	...	...	...	...	0.97
NGC 1079	2.2	5.60	0.73	7	65	34.6	0.51[b]	72	...	...	...	...	0.26
NGC 1317	2.1	5.33	0.94	53	11	26.1	0.63[b]	64	0.22[b]	36	0.85[c]	36	0.34
NGC 1326	3.0	7.00	0.99	21	15	36.8	0.28[b]	42	0.74[b]	28	...	...	0.34
NGC 1350	2.2	8.31	0.71	13	57	141.4	0.53[d]	43	...	...	...	...	0.25
NGC 1387	1.8	4.41	0.96	54	72	29.6	0.36[b]	55	...	...	...	...	0.39
NGC 1411	1.9	0.72	0.88	10	4	18.2	0.80[e]	15	...	...	...	...	0.08
NGC 1512	1.2	4.78	0.82	70	77	36.9[f]	...	...	...	...	...	...	...
NGC 1533	1.5	3.88	0.90	39	10	25.3	0.41[b]	29	0.85[g]	29	...	...	0.25
NGC 1553	1.9	8.51	0.72	155	...	50.1	0.93[h]	100	...	...	...	...	0.21
NGC 1574	2.9	6.51	0.97	31	24	34.4	0.38[b]	8	0.89[g]	8	...	...	0.38
NGC 3081	2.1	1.53	0.68	19	60	21.1	0.51[b]	41	0.88[d]	21	...	...	0.10
NGC 3100	...	...	...	...	...	28.7	0.74[c]	16	...	...	...	...	...
NGC 3706	3.6	39.40	0.67	1	...	1.4	...	...	...	...	...	...	0.92

Notes.—Here fii_1 is the deviation of ϕ_{bulge} from the orientation of the outer disk, whereas fii_2 is the deviation of ϕ_{bulge} from the orientation of the primary bar. The fii value for the other three components is the orientation of the component with respect to the outer disk.
[a] Inner disk.
[b] Bar.
[c] Oval fitted by Sérsic function.
[d] Bar + oval could not be fitted separately.
[e] Middle disk fitted by Sérsic function.
[f] Bar + disk could not be fitted separately.
[g] Oval fitted by Ferrers function.
[h] Oval fitted by Ferrers function with $n = 1$.

linked to an outer Lindblad resonance (Buta & Crocker 1991). This feature includes a well-defined outer ring from which two conspicuous spiral arms emerge. Sandage & Brucato (1979) also recognized NGC 1079 as an early-type spiral. The bar in NGC 1079 was recognized by Jungwiert et al. as a large peak at $r = 30''$ in the ellipticity profile, while a smaller peak at $r = 17''$ was attributed to a triaxial bulge. We see both peaks in our ϵ-profile as well. The axis ratio of the disk ($q = 0.59$) deviates from the axis ratio of the bulge ($q = 0.68$), confirming that they are separate components.

In our decomposition we first determined h_r, which was then kept fixed. Finally, the bulge, disk, and bar were fitted, but for the ansae-type morphology of the bar the solution depends slightly on the parameters of the bar: it is possible to use $n > 2$ or $n = 2$ together with a shape parameter that deviates from purely elliptical isophotes. Depending on this choice, we found $B/T = 0.20$–0.25. Our solution converges only if flattening of the bulge is taken into account. The bar has a high surface brightness compared to that of the underlying disk. Apparently, an inner ring surrounds the bar, seen as a residual after subtracting the model image from the observed image.

Our solution for this galaxy is very different from the 2D bulge/disk solution obtained by SGA04. They found a large de Vaucouleurs–type bulge ($B/T = 0.65$, $n = 3.82$) dominating the whole surface brightness profile and a very weak exponential inner disk extending to the radius of the bar. In their fit the disk at the edge of the bar is about 5 mag weaker than the bulge. SGA04 made the decomposition in the R band, which extends approximately to the same radial distance as our K_s-band image. For comparison, we also made a 2D bulge-disk decomposition (thus omitting the bar), which gives $B/T = 0.57$ (see Fig. 6, *top right*). This is near the B/T ratio obtained by SGA04, except that the bulge is more exponential ($n = 2.7$). However, we stress that in this solution the flux of the bar goes erroneously to the bulge. A

similar solution was found by us using the 1D method. This resembles the solution by SGA04 even more, although the disk we find is still several magnitudes brighter than that obtained by SGA04. It is also possible to find a solution in which the surface brightness profile is fitted by a single Sérsic function with $n = 3.3$ (Fig. 6, *top middle*), but in that case the fit is not good, and, in particular, the model image is very different from the original image.

NGC 1317: NGC 1317 has been previously reported to be a double-barred galaxy, both in the optical (Schweizer 1980; Wozniak et al. 1995) and in the near-infrared (Mulchaey et al. 1997). The galaxy also has a nuclear ring, which is actually a double ring/pseudoring evident particularly in blue light (Schweizer 1980; Papovich et al. 2003) and in Hα (Crocker et al. 1996). The galaxy is nearly in face-on orientation. For the disk, RC3 gives a larger ellipticity than is found in this study, most probably because the outer isophotes are elongated toward the nearby companion.

The secondary bar is clearly visible in our K_s-band image, and the double nuclear ring is now detected for the first time also in the near-infrared. The outer structure is dominated by a large oval with no clear sign of a primary bar. However, after subtracting the exponential disk a very weak classical bar becomes visible (see Fig. 5). Previous evidence for the primary bar comes from the ϵ-profiles, which are largely associated with the large oval. The secondary bar lies within a bright nuclear lens (first noticed by Schweizer 1980) and is completely detached from the nuclear ring/pseudoring. Together, the secondary bar and its lens appear as a bump in the radial surface brightness profile. In the decomposition only one primary component was fitted. For the complex structure of this galaxy the decomposition was made in small steps. The parameters for the disk and the main bar/oval were found first, after which they were fixed. Then the secondary bar was found and fixed, and finally the bulge component was found. In the central part of the galaxy the secondary bar dominates the
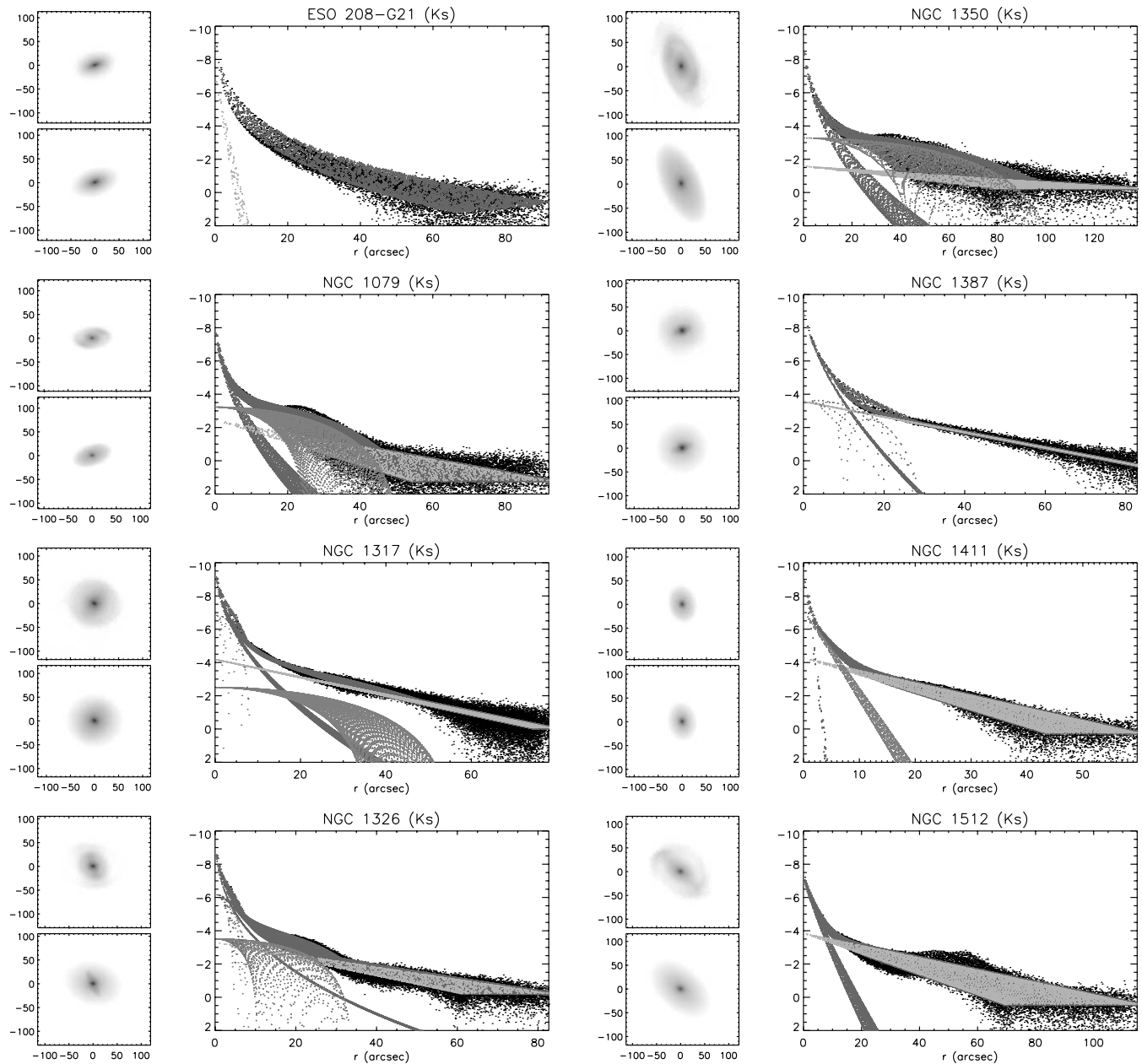
Fig. 4.—Multicomponent decompositions in the K_s band (except for NGC 3100 in the J band). For each galaxy we show the observed image (*upper left of each panel*), the image constructed from the model functions (*lower left of each panel*), and the μ-profile together with the fitted model functions (*right of each panel*); r gives the distance to galaxy center in the sky plane. The observed μ-profile is shown by black dots. The disk is shown by light gray, bars by medium gray, and the complete model and the bulge by dark gray. The zero point of the surface brightness is arbitrary but selected so that 1 unit corresponds to 1 mag. In order to reduce the image size only a fraction of the pixel values are shown in the plots.

central oval, and therefore it is the component that the fitting procedure found. In the final solution all components (except the shape parameter of the bar) were left free for fitting. The solution we find is reasonable, although it leaves some residuals, mainly because the bars and ovals cannot be fitted separately.

The double nuclear ring in the $J - K_s$ color map shows the presence of dust, which is consistent with the observation that the ring is currently forming stars. The ring and the secondary bar are also clearly visible in the K_s-band image after subtracting the bulge (Fig. 5). The ring has a patchy morphology, possibly indicating the presence of red supergiants. Also, there are dust lanes in the central regions of the galaxy that are not aligned with the secondary bar.

NGC 1326: This is a well-studied galaxy previously reported to have a primary bar, a possible nuclear bar, and inner and outer rings. The outer ring is an exceptionally bright example of the outer Lindblad resonance subclass R_1, characterized by an approximate alignment perpendicular to the bar and by slight dimpling in its shape near the bar axis (Buta & Crocker 1991). The nuclear ring is also an exceptional star-forming feature that has been well studied from both ground and space (Buta & Crocker 1991; Garcia-Barreto et al. 1991; Storchi-Bergman et al. 1996; Cid Fernandes et al. 1998; Buta et al. 2000). The inner bar and the inner and outer rings are visible in our K_s-band image, and the nuclear ring is evident in the $J - K_s$ color map. We detect a faint secondary bar inside the nuclear ring, which is most visible in the
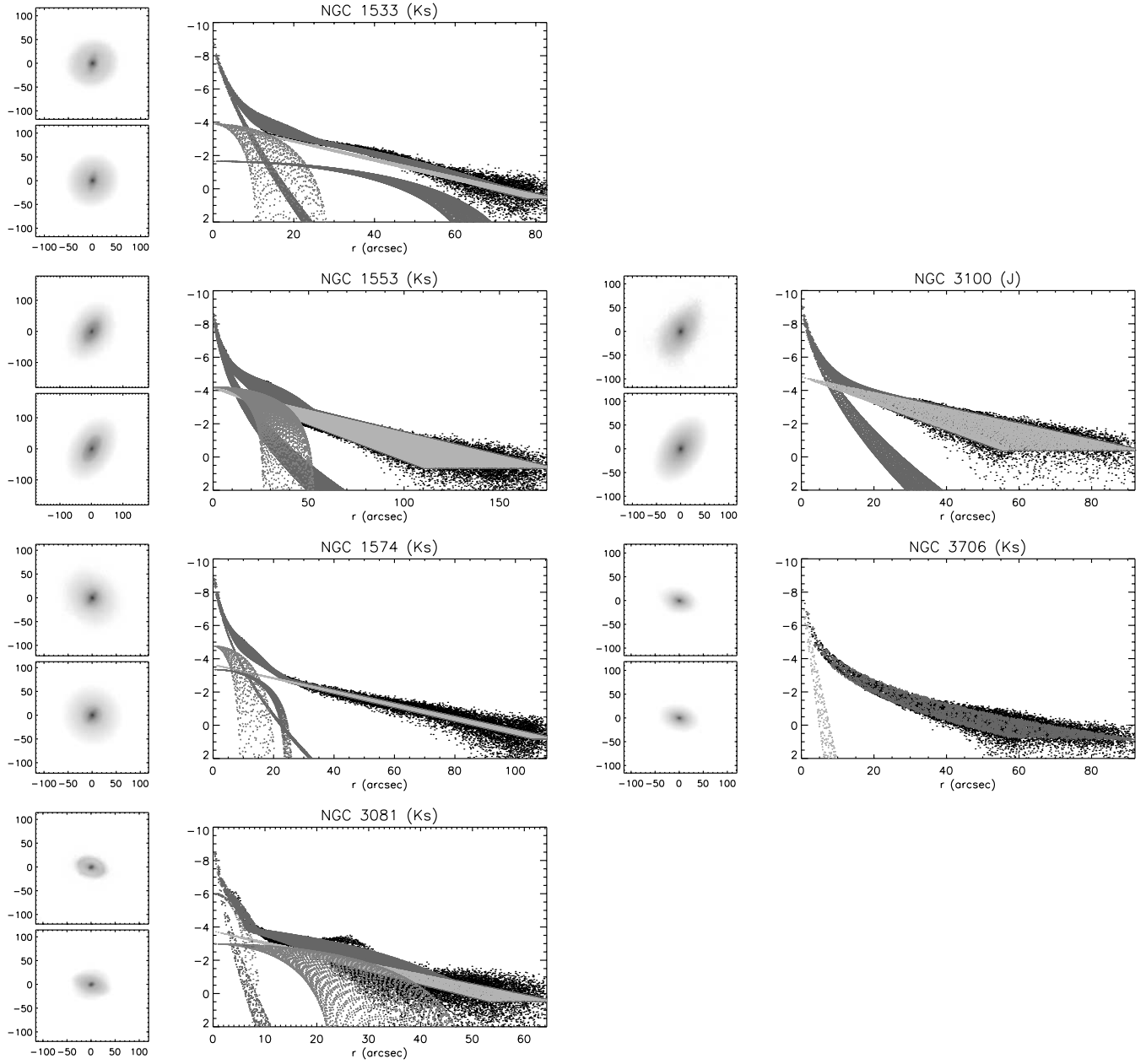
Fig. 4.—Continued

TABLE 5
IDENTIFICATION OF THE STRUCTURAL COMPONENTS

Galaxy	Identifications
ESO 208-G21	Bulge, inner disk
NGC 1079...................................	Bulge, disk, bar, extended oval
NGC 1317...................................	Bulge, disk, bar_1, bar_2:, $oval_1$, $oval_2$
NGC 1326...................................	Bulge, disk, bar_1, bar_2, $lens_1$, $lens_2$
NGC 1350...................................	Flattened bulge or lens, disk, bar
NGC 1387...................................	Bulge, disk, bar, lens
NGC 1411...................................	Bulge, middle disk, outer disk
NGC 1512...................................	Bulge, disk, bar, oval
NGC 1533...................................	Bulge, disk, bar, lens, inner ring
NGC 1553...................................	Bulge, disk, lens, inner disk
NGC 1574...................................	Bulge, disk, bar, lens
NGC 3081...................................	Bulge, disk, bar_1, bar_2, lens
NGC 3100...................................	Middle disk, outer disk
NGC 3358...................................	Bulge, disk, bar_1, bar_2, oval
NGC 3706...................................	Bulge, inner disk

NOTES.—Rings are excluded; these are presented in Table 6. The colon indicates uncertainty.

TABLE 6
MAJOR-AXIS RING DIMENSIONS

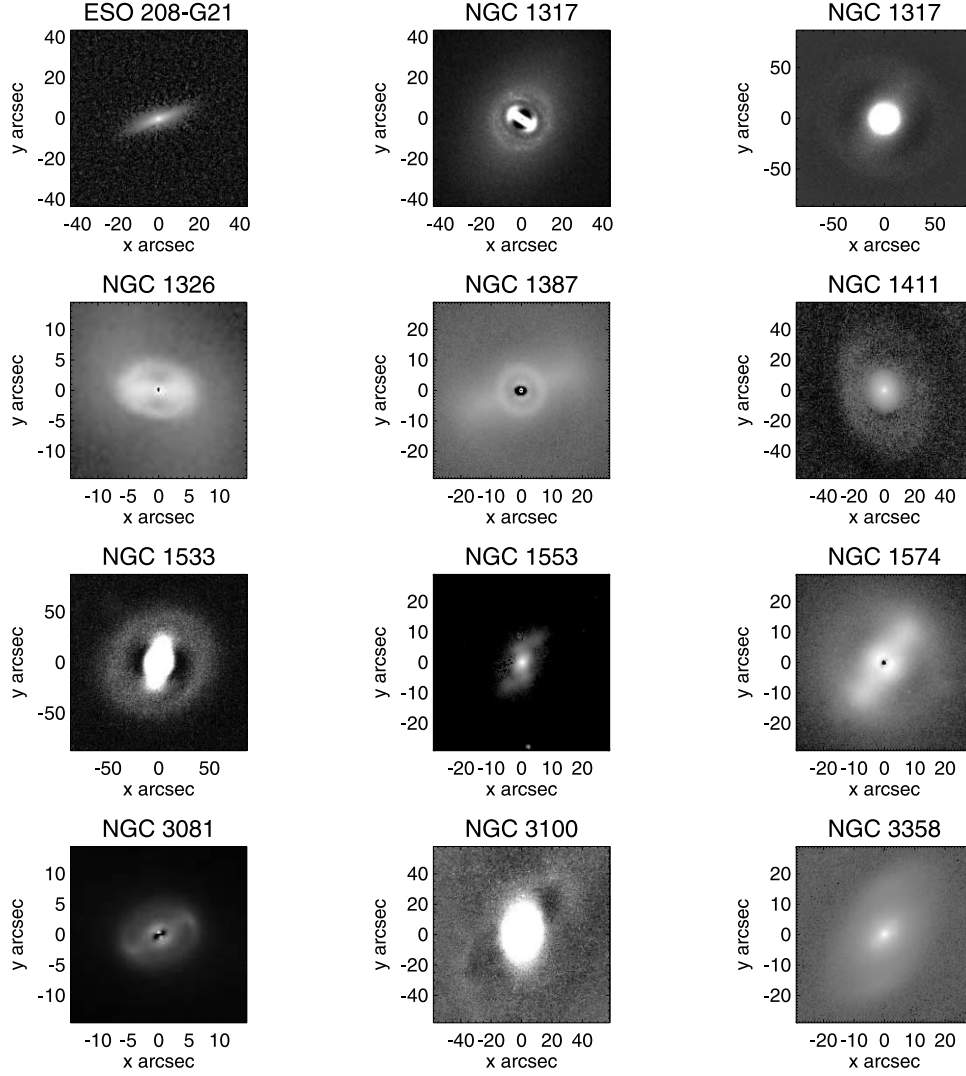| Galaxy	Nuclear (arcsec)	Inner (arcsec)	Outer (arcsec)
NGC 1079........................	. . .	15	. . .
NGC 1317........................	7, 13	53	94
NGC 1326........................	6	28	71
NGC 1350........................	. . .	80	170
NGC 1387........................	6	. . .	. . .
NGC 1411........................	. . .	37	. . .
NGC 1512........................	8	64	. . .
NGC 1533........................	. . .	44	. . .
NGC 1574........................	. . .	17	. . .
NGC 3081........................	7	33	57
NGC 3100........................	. . .	. . .	. . .
NGC 3358........................	. . .	22	. . .

Fig. 5.—Residual images for nine of the galaxies in the sample. For ESO 208-G21 an unsharp mask image is shown (a smoothed image subtracted from the original image), and for galaxies NGC 1411, NGC 1533, and NGC 3100 the exponential disk obtained from the decomposition is subtracted from the original image, whereas for the rest of the galaxies the bulge component is subtracted. For NGC 1317 both bulge- and disk-subtracted images are shown (*top middle and top right, respectively*). Only the inner regions of the galaxies are shown.

K_s-band image after subtracting the bulge model (Fig. 5). The possible double-barred nature of NGC 1326 was previously discussed by de Vaucouleurs (1974), Buta & Crocker (1991), Wozniak et al. (1995), and Erwin (2004), but it has been difficult to verify owing to strong extinction inside the nuclear ring. The best evidence presented previously was by Erwin (2004), but the resolution in our K_s-band image is sufficient now to confirm it. The $J - K_s$ color index map in Figure 1 shows that dust still has some impact in the near-infrared bands inside the nuclear ring. The ring is red in this map, which suggests the presence of red supergiants.

In our decomposition for NGC 1326, in addition to the bulge and the disk we also fitted two bars. This solution converges only if the flattening of the bulge is taken into account. Models for the individual components were found in small steps, and finally all components were fitted simultaneously. The bulge in this galaxy was found to be quite prominent ($B/T = 0.34$, $n = 3.0$) but much less luminous than argued by SGA04. They found a very weak extended disk embedded inside a large de Vaucouleurs–type bulge dominating the whole surface brightness profile, leading to $B/T = 0.63$ and $n = 4.9$. For comparison, we also made bulge-disk-bar

and bulge-disk decompositions, the former leading to $B/T = 0.42$ and the latter to $B/T = 0.58$ (and $n = 3.1$) (see also Fig. 6). However, in the bulge-disk decomposition the flux of the bar/oval goes erroneously to the bulge. It is also worth noting that the B/T in the bulge-disk-bar decomposition is somewhat larger than in the decomposition in which two bars were fitted ($B/T = 0.42$ vs. 0.34), which means that in this case even the bar/oval (visible as a bump at $r = 5''$–$10''$ in the μ-profile) affects the solution.

NGC 1350: This galaxy has been previously reported to have a prominent inner ring and an outer pseudoring of type R'_1 (Crocker et al. 1996). In the B band, NGC 1350 shows a prominent inner ring and an outer Lindblad resonance subclass R'_1 pseudoring (Buta & Crocker 1991). In the K_s band, NGC 1350 shows similar features. The galaxy also shows a clear ansae-type bar, both in the direct images and in the ϵ-profile. The bar is more conspicuous at 2.2 μm than in blue light, but it is still relatively weak. Internal extinction masks much of the bar in blue light. There is no clear sign of a secondary bar, but a peak appears in the ϵ-profile at $r = 8''$, associated with an isophotal twist, which at least indicates that a separate structural component exists at that radius. It might be an inner disk, because the orientation deviates by only $13°$ from
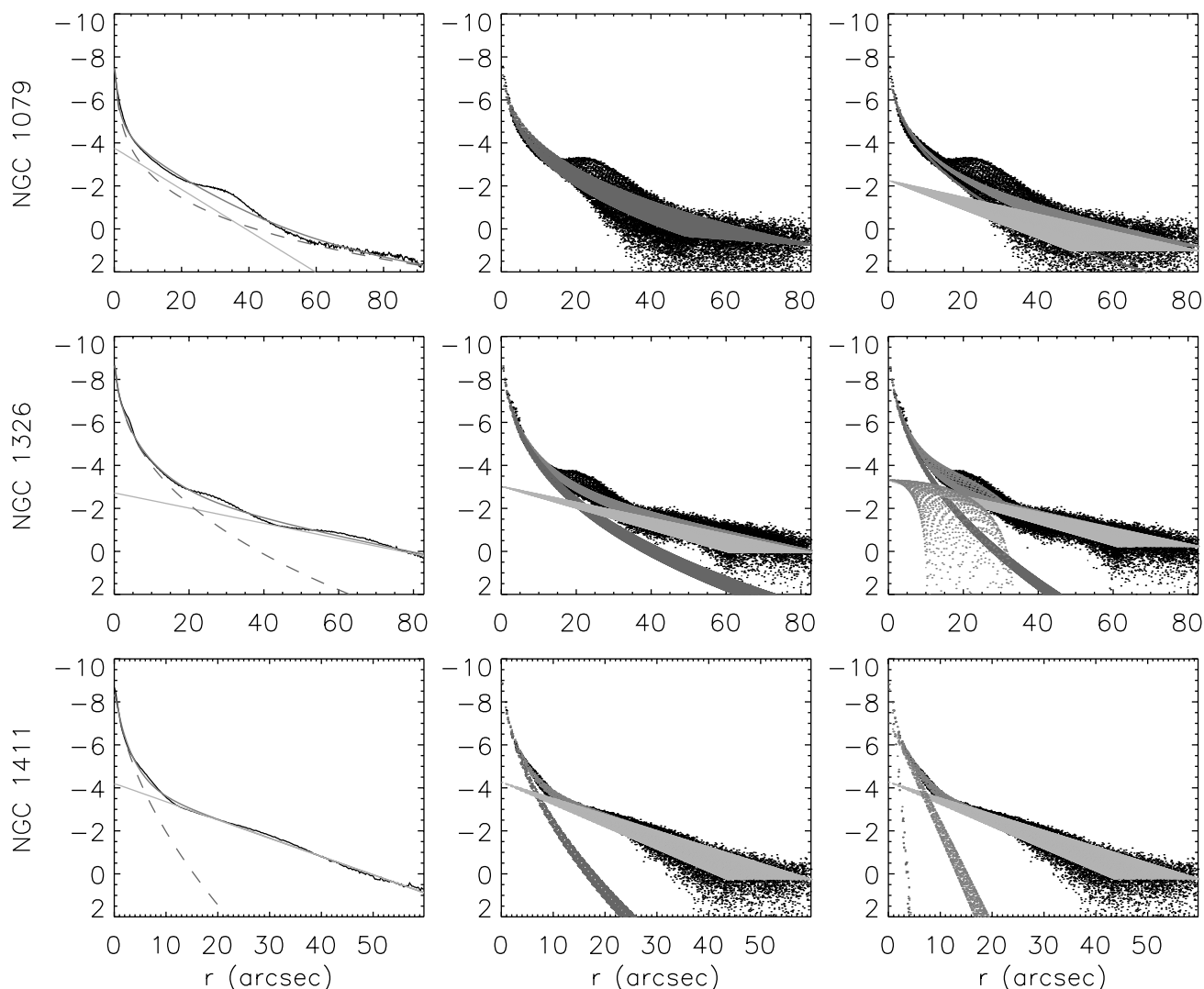
the orientation of the outer disk. The bulge has a different orientation than the bar, so in our decomposition the two components cannot be mixed.

The different components in the decomposition were found in small steps, and in the final solution the parameters of the disk and the length of the bar were fixed, the latter because for the ansae-type morphology the model would otherwise overestimate it. Again, in the simple 2D bulge-disk decomposition the flux of the bar goes erroneously to the bulge, giving $B/T = 0.77$, instead of $B/T = 0.25$, obtained in our best-fitting solution. For this galaxy the flattening of the bulge is high ($q = 0.71$).

NGC 1387: This galaxy is an excellent example of a very early type barred galaxy. Although classified as type SAB in RC3, Pahre (1999) and BCO06 adopted an SB type. The Q_b family from Paper II is AB, indicating that the bar is indeed weak. NGC 1387 has no spiral arms, but the surface brightness profile at $r = 30''$–$90''$ is perfectly exponential, which is a strong sign of a disk.

In the decomposition we fitted, besides the bulge and the disk, the bar/lens for which one single function was used. Subtraction of the bulge model from the original image showed that this galaxy has a prominent nuclear ring at $r = 6''$ (Fig. 5), which also

appears as a faint peak in the ϵ-profile (Fig. 2). The ring is nearly circular and has a significant size compared to the length of the bar. In the surface brightness profile the bulge and the disk appear as two nearly exponential functions.

NGC 1411: Sandage & Bedke (1994) noticed that NGC 1411 has a three-zone structure with a ring between the second and the third components. BCO06 noted a series of lenses and classified it as type SA(l)0° based on a V-band image. In our K_s-band image, only the innermost lens clearly stands out, but a weak outer lens, which actually has the appearance of a smooth ring, can also be detected in Figure 5 after subtracting the exponential disk. The surface brightness profile of this galaxy shows three nearly exponential parts in the K_s-band image.

In spite of the simple-looking profile, it was not easy to find a solution that converged. Again, the solution was found in small steps so that robust solutions for the two inner components were found first. They were fixed, and a solution for the outer disk was found. After that, the parameters of the outer disk were fixed, and more precise solutions were found for the two inner components. Finally, all parameters of the bulge and the middle component were left free for fitting. The bulge and the middle component were fitted using a Sérsic function, whereas for the outer disk an exponential

function was used. Our decomposition confirms the visual impression that all three components are nearly exponential. We found $B/T = 0.08$, which is as small as the typical B/T ratios in Sc-type spiral galaxies. Our value for NGC 1411 is not essentially larger than the $B/T = 0.11$ found in Paper I for Sc galaxies using the same decomposition method. A similar small B/T ratio of 0.15 for Sc galaxies is also given by Binney & Merrifield (1998) based on the R-band measurements by Kent (1985). NGC 1411 might therefore be a genuine example of an S0c galaxy, that is, the proverbial analog of an Sc galaxy in a classical S0, as discussed in the DDO galaxy classification scheme by van den Bergh (1976, 1998).

A two-component robust 2D bulge-disk decomposition gives $B/T = 0.39$. In this solution the B/T value is very large because the two inner exponentials are fitted by a single Sérsic function. For this galaxy the 1D decomposition (see Fig. 6, *bottom left*) gives a solution very similar to the 2D bulge-disk decomposition (*bottom middle*). In its simplicity NGC 1411 is an illustrative example: it clearly demonstrates that if a three-component galaxy is fitted by a two-component model, the two-dimensionality alone does not automatically improve the result.

NGC 1512: This is a well-known interacting system and one of the latest Hubble types in our sample. The morphology is dominated by a strong bar and two rings: a bright oval inner ring around the bar ends and an intense nuclear ring in the center of the bar. A deep B-band *Spitzer* Infrared Nearby Galaxies Survey Legacy image (Kennicutt et al. 2003) also reveals a distorted outer ring, as well as faint tidal debris near the companion NGC 1510. The nuclear ring was first noted by Hawarden et al. (1979), who also showed the extent of NGC 1512's interaction with the neighboring NGC 1510. Jungwiert et al. (1997) noticed an isophotal twist at $r = 7''$, which was suggested to be due to a triaxial bulge. However, Erwin (2004) used *HST* NICMOS images to show that the twist is due to the nuclear ring, with no evidence of a bar inside the ring (see also de Grijs et al. 2003). The ring (with no bar inside) is clearly visible in our K_s-band image and in the $J - K_s$ color index map. As is typical of such rings, the morphology is patchy and indicative of strong star formation (Maoz et al. 2001).

As our image is not deep enough for a reliable decomposition for this galaxy and the position angle is very uncertain, we give only a rough estimate of the relative mass of the bulge. Only two components are used, a Sérsic function for the bulge and an exponential function for the bar + disk. The bulge has nearly circular isophotes and is fitted by a function that approaches an exponential ($n = 1.2$), thus indicating the disklike nature of the bulge. However, we stress that the decomposition is very uncertain, and therefore, no B/T flux ratio is given in Table 4.

NGC 1533: BCO06 classify the galaxy as type (RL)SB0°, implying a large ring/lens outside the bar, but one that is not similar to rings/ovals generally found for early-type galaxies. Sandage & Bedke (1994) noticed the slight enhancement at the rim of the RL and classified the galaxy as an SB0$_2$/SBa. Sandage & Brucato (1979) also noted the large lens underfilled by the bar, and they also suspected a weak spiral pattern in the outer lens.

For this galaxy it was possible to fit the bar and the lens separately. However, it was more difficult to find h_r, mainly because the lens dominates the disk in our image. Therefore, h_r was found using the 1D method by fitting an exponential to the outer disk. In the 2D decomposition, h_r was fixed to this value.

NGC 1553: The dominant feature of this galaxy's morphology is a strong inner ring/lens (Sandage & Brucato 1979; Kormendy 1984). The lens shows subtle structure in our K_s-band image and is classified as an inner ring in RC3. BCO06 give a type of SA(rl)0$^+$

to highlight that the feature really is more a ring than a lens. In the central part of the galaxy a second elongated feature is present, which in our unsharp mask (Fig. 5) appears to be a nuclear disk showing spiral arms. Sandage & Bedke (1994) noticed that this galaxy has subtle dust lanes in the disk, leading to its classification as a peculiar SB0/Sa. The major-axis rotation curve for this galaxy is found to be typical for S0 galaxies (Kormendy 1984; Rampazzo 1988). Contrary to all previous evidence, SGA04 reclassified NGC 1553 as an elliptical with an inner disk, a choice that was justified by the fact that their decomposition did not find any outer disk. No B/T ratio is given by SGA04, but the shape parameter of the bulge was found to be $n = 5.24$.

In our analysis the presence of the inner disk is obvious: it is particularly clearly visible in the image in which the exponential disk is subtracted, shown in Figure 5. The best 2D solution was found by fitting a bulge, lens/ring, and an outer disk, which appeared to be exponential (as in the μ-profile by Kormendy 1984). We found $B/T = 0.21$ and $n = 1.9$. Again, in order to duplicate the 2D solution of SGA04 we also made a 2D bulge-disk decomposition; this gives $B/T = 0.88$ and $n = 3.33$, which is exactly the same result as that obtained by our 1D method for this galaxy. The reason for the very large difference between our two- and three-component decompositions is that in the two-component solution the flux of the lens goes erroneously to the bulge. In all our decompositions the shape parameter of the bulge is considerably smaller than the value $n = 5.24$ obtained by SGA04.

The nature of the bulge in this galaxy is unclear even in our best-fitting solution. The component that is fitted as a bulge is actually the inner disk, and there is no other more spherical component in the central regions that could be interpreted as a bulge. Perhaps there is no bulge in this galaxy, unless the inner disk is interpreted as a pseudobulge. Kinematical evidence for this interpretation comes from the study by Kormendy (1984), who argued that the bulge (the small central component) is cooler than the lens that dominates at larger radial distances. The change in the stellar velocity dispersion occurs at $r = 12''–15''$, after which the lens starts to dominate. This is precisely the distance inside of which we find the disklike bulge in our decomposition.

NGC 1574: BCO06 classify this galaxy as type SB0$^-$, where the bar is a well-defined feature embedded in a huge extended disk component. The bar was also noted by Sandage & Bedke (1994) but was missed in RC3. De Vaucouleurs & de Vaucouleurs (1964) pointed out the presence of a lens. Although Sandage & Bedke note that NGC 1574 has a three-zone structure typical of S0 galaxies, BCO06 could not identify a clear inner lens around the bar. From our K_s-band image it is difficult to judge for sure whether this galaxy has a lens or not, but the surface brightness profile shows three nearly exponential parts, which is the case also in some other galaxies with lenses in our sample. The bar is embedded inside the middle exponential component of the disk.

The decomposition was carried out starting from the parameters of the outer disk. Once reasonable approximations were found for all components, better solutions were searched for separately for each of them. Finally, all parameters describing these components (except for the ellipticity of the lens) were left free for fitting. Contrary to the usual case, for this galaxy the decomposition depends critically on the image resolution: by rebinning the image by a factor of 4, we find $B/T = 0.28$ and $n = 1.5$, whereas for the original image we obtain $B/T = 0.38$ and $n = 2.9$. A possible reason for the large difference between these two solutions is the compact central cusp at $r = 9''$, found by Phillips et al. (1996): most probably the cusp is better resolved in the original image. The fitted lens inside the bar region mainly improves the model image but does not affect the properties of the bulge. Subtracting

the bulge model from the original image shows a complete inner ring surrounding the bar, which changes the RC3 s-variety classification to r-variety.

NGC 3081: NGC 3081 is a well-known Seyfert 2 galaxy having four exceptionally well-defined rings (Buta & Purcell 1998): an R_1 outer ring intrinsically aligned nearly perpendicular to the bar, a nearly circular R_2' outer pseudoring, a highly elongated, aligned inner ring, and a misaligned nuclear ring. The deprojected radii of these features are $90''$, $105''$, $35''$, and $14''$, respectively, and color index maps (Buta 1990; Buta & Purcell 1998) indicate that each ring is a well-defined zone of active star formation. The strong similarity between these rings and test-particle models of barred spiral galaxies (Simkin et al. 1980; Schwarz 1981) led Buta & Purcell (1998) to classify NGC 3081 as a resonance-ring galaxy. The galaxy also has a complex double-barred structure detected both in the optical and in the near-infrared (Buta 1990; Friedli et al. 1996; Mulchaey et al. 1997; Erwin 2004; Laine et al. 2002). The primary bar is a weak feature that underfills the bright inner ring. The secondary bar lies within the nuclear ring and is misaligned with the primary bar by $71°$. Except for the R_2' outer pseudoring, all of these structural components of NGC 3081 are visible in our K_s-band image. The secondary bar is also surrounded by a lens extending to the radius of the nuclear ring. As noted in Paper II, the main barlike feature in NGC 3081 is the massive oval rimmed by the inner ring. The apparent primary bar underfills this ring/oval and seems insignificant in comparison. In spite of its early morphological type (S0/a), NGC 3081 has $J - H$, $H - K$, and $K - L'$ colors similar to those typically found in spiral galaxies (Alonso-Herrero et al. 1998). The hydrogen index also indicates a higher than average H I content for its type (Buta 1990). Star formation in the nested rings has also been studied by Ferruit et al. (2000), Buta et al. (2004), and Martini et al. (2003), although in the circumnuclear regions (210–590 pc) the stellar population is largely dominated by old stars (Boisson et al. 2004). Buta et al. (2004) show high-resolution *HST* images of the inner regions of NGC 3081, revealing hundreds of barely resolved star clusters in the inner ring. The distribution of these clusters belies the intrinsic oval shape of the ring because they concentrate in arcs around the ring major axis. Evans et al. (1996) also noted that NGC 3081 has a bright nucleus with an apparent bulge visible to a radius of $r = 10''$.

In the decomposition we fitted the bulge, disk, secondary bar/lens, and primary bar. It was difficult to find a solution that converges, which is not surprising taking into account the rich morphology of this galaxy. As always in complicated cases, a reasonable solution was found by repeating a series of decompositions. In the inner regions it was not possible to simultaneously fit the bulge, lens, and secondary bar, mainly because of the presence of the strong nuclear ring. Instead, a solution was found in which the nuclear bar and the lens were fitted by a single function. Also, the simultaneous presence of a weak primary bar and a strong ring leads to a solution in which the bar fills the region up to the radius of the inner ring. This somewhat overestimates the flux of the primary bar. However, this is not expected to seriously underestimate the flux of the bulge, which resides in the central regions of this galaxy. In the residual image both the inner and the nuclear ring are clearly visible, and the secondary bar shows an ansae-type morphology.

NGC 3100: In the early work by Sandage & Brucato (1979), weak spiral arms were detected in the outer disk, although in RC3 this galaxy is classified as a weakly barred peculiar S0. In our analysis NGC 3100 appears as a system with a large lens and a bright nuclear component, which de Vaucouleurs & de Vaucouleurs (1964) already paid attention to. Evidently, there are also weak

asymmetric spiral arms in the outer disk, as demonstrated by the image in which the disk model is subtracted (Fig. 5). The bulge component is difficult to evaluate in this galaxy. It could be the bright nuclear component, or perhaps there is no bulge at all. The larger component fitted by a Sérsic function is clearly the large lens having an n-parameter ($n = 1.8$) typical for disky systems. As we were not able to fit the small nuclear component, no B/T ratio is given in Table 6. This is our second candidate of galaxies that might be an analog of late-type spirals among S0 galaxies.

NGC 3358: The surface brightness of this early-type spiral $[(R_2')\mathrm{SAB}(\mathrm{l})a]$ is high, and the main morphological features lie on an extended, almost flat distribution of light. The galaxy is most noteworthy for its strong R_2' outer pseudoring, which is made from two bright arms that begin well off the ends of the bar and which partly overshoot those ends. The overshoot indicates a trace of an R_1 component. In optical images, the outer pseudoring is lightly patchy and is affected by dust lanes on the near side. The bar is a weak ansae type but also has some characteristics of spiral arms (see Fig. 5). The bar is embedded in a well-defined inner lens, which causes conflicting interpretations of the variety. There is a trace of a secondary bar in our K_s-band image, previously detected in the optical region by Buta & Crocker (1993; see also Erwin 2004). The bulge seems to be the very small, nearly spherical component inside the secondary bar. Unfortunately, the structure of this galaxy was too complicated for any reasonable decomposition. Because of the Freeman type II surface brightness profile, not even a 1D decomposition was made.

NGC 3706: This galaxy seems to have a very small, nearly edge-on inner disk embedded inside a prominent bulge. The inner disk has been directly detected in the *HST* image (filter F555W) by Lauer et al. (2005), being visible above the bulge to at least $r = 1''$. They also found a stellar ring at that radius. It is possible to fit this galaxy either by a single de Vaucouleurs–type function or by adding an exponential inner disk. The two-component solution gives a marginally better fit and, above all, it better represents the preidentified structural components of this galaxy. In that case the shape parameter of the bulge is also more reasonable: $n = 3.6$ instead of $n = 5.1$. Our best solution is very similar to that found by Scorza et al. (1998) in the V band; in both cases $B/T = 0.92$ was found (Scorza et al. give $D/B = 0.06$). As in our K_s-band image, a subtle trace of an inner lens is visible; we interpret the galaxy as type E^+4.

5.4. *A Comparison of 1D and 2D Decomposition Results*

It is generally assumed that bars in 2D decompositions do not affect the relative masses of bulges or the properties of bulges and disks, an understanding that is largely based on the study by de Jong (1996), who compared 2D bulge-disk and bulge-disk-bar decompositions for spiral galaxies. Later it was shown by Peng et al. (2002) for a few individual galaxies and in Paper I for a larger number of early-type disk galaxies that bars might actually play an important role in the structural decompositions. These studies applied more advanced 2D methods than were used in the study by de Jong. In particular, it was shown in Paper I that the omission of a bar might overestimate the mass of the bulge even by 40%. Another generally accepted assumption is that 2D methods always give more reliable results than 1D methods. In the following we evaluate the reliability of this assumption.

The mean values for the parameters of the bulge and the disk were calculated by including in the statistics all those 13 galaxies in our sample for which it was possible to estimate the B/T ratio in a reasonable manner (excluded are NGC 3358 and NGC 3100),

TABLE 7
MEAN B/T RATIO AND n_{bulge} AS ESTIMATED USING THE 1D
AND 2D DECOMPOSITIONS

Method	$\langle B/T \rangle$	$\langle n_{\text{bulge}} \rangle$	$\langle h_r \rangle$
All ($N = 13$)			
2D (final)	0.39 ± 0.07	2.4 ± 0.2	34.7
2D (bulge-disk-bar)	0.40 ± 0.07	2.3 ± 0.2	34.7
2D (bulge-disk).....................	0.61 ± 0.07	2.8 ± 0.2	34.7
1D..	0.55 ± 0.06	2.9 ± 0.4	25.9
Disk-dominated ($N = 11$)			
2D (final)	0.25 ± 0.03	2.1 ± 0.1	38.5
2D (bulge-disk-bar)	0.30 ± 0.03	2.1 ± 0.1	38.5
2D (bulge-disk).....................	0.55 ± 0.06	2.6 ± 0.1	38.5
1D..	0.48 ± 0.04	2.7 ± 0.4	30.2

NOTE.—The errors are the errors of the mean.

as well as the 11 disk-dominated systems. The results are shown in Table 7. A comparison of 2D two- and three-component decompositions shows that when the primary bars or ovals are omitted, the B/T ratios are significantly overestimated, mainly because the flux of the third component goes erroneously to the bulge. Also, in the three-component decompositions the bulges are more exponential than those obtained using the two-component method. However, including more components to the fit does not affect the mean B/T ratio considerably. Multiple bars/ovals affect the B/T ratio only in galaxies with very small bulges or high surface brightness secondary bars or ovals. Our best-fitting multicomponent method gives $\langle B/T \rangle = 0.25$ and $\langle n \rangle = 2.1$, which are very similar to the $\langle B/T \rangle = 0.24$ and $\langle n \rangle = 2.1$ found earlier in Paper I for a sample of 24 northern early-type disk galaxies. This B/T flux ratio is considerably smaller than obtained by our 2D bulge-disk approach, which gives $\langle B/T \rangle = 0.55$. If the two elliptical galaxies classified as S0 by SGA04 are also included, $\langle B/T \rangle = 0.61$. This is very similar to the mean B/T ratio of 0.61 obtained by SGA04 using a similar 2D bulge-disk decomposition approach in the same wavelength.

We also find that h_r is not sensitive to the 2D method used, indicating that a bar or an oval does not affect the scale length of the disk. The 1D method generally gives similar h_r, but there are some individual cases for which different h_r values are obtained. The 1D method failed to find the extended disks for the galaxies NGC 1079 ($h_r = 14''$ vs. $34''$) and NGC 1350 ($h_r = 47''$ vs. $141''$). For NGC 3081 the 1D method gives larger h_r ($38''$ vs. $21''$), mainly because the 1D fit extends to a larger radial distance. Therefore, in this case the 1D method gives a more reliable estimate of h_r. It is these exceptional cases that cause the small difference in the mean h_r obtained by the 1D and 2D methods in Table 7. In conclusion, we did not find any evidence supporting the view that for multicomponent galaxies the 2D method automatically gives better results than the 1D method. This is the case only if, in addition to the bulge and the disk, at least one more component is included in the 2D fit.

6. THE NATURE OF BARS AND BULGES IN EARLY-TYPE DISK GALAXIES

For any hypothesis of galaxy evolution it is important to understand whether bulges in galaxies are old, classical bulges or pseudobulges formed at later phases of galaxy evolution. The main approaches for evaluating this are the kinematic and photometric approaches. Bulges are expected to have the character-

istics of pseudobulges mainly when $n < 2$ (KK04). This might also be the case when the bulge is oriented near the plane of the outer disk or the ellipticity of the bulge is near that of the outer disk. However, the bulge is not necessarily aligned with the disk. The S0 class might have many disks with different orientations, of which NGC 1411 is a good example. It is also assumed by KK04 that if a galaxy has a secondary bar or a nuclear ring inside the bulge, the bulge is most probably a young pseudobulge. Even more direct evidence for the existence of a pseudobulge can be obtained kinematically: if the ratio of the maximum velocity amplitude (V_{max}) to the mean stellar velocity dispersion (σ) at the same radius, V_{max}/σ, versus the ellipticity (ϵ) is above the isotropic oblate rotator curve (Binney 1980), the bulge is kinematically supported. This means that stars of the bulge have not had time to gain such large random velocities as in the case of older classical bulges. Unfortunately, useful kinematic data are available only for a few galaxies in our sample.

We found strong evidence of pseudobulges in the nonelliptical galaxies in our sample. The shape parameter of the bulge is smaller than 2 in six of the 12 galaxies and near $n = 2$ in 10 of the galaxies. For NGC 3358 no decomposition could be made, but, as discussed above, the bulge for this galaxy is very small and most probably has the characteristics of a pseudobulge. Larger n-values for the bulge were detected only for NGC 1326 ($n = 3.0$) and NGC 1574 ($n = 2.9$), but even NGC 1326 has a nuclear star-forming ring, and for NGC 1574 there is strong kinematic evidence showing that the bulge is rotationally supported. For NGC 1574 we use σ and V_{max} as measured by Jarvis et al. (1988). They found $V_{\text{max}}(\text{obs}) = 40$ km s^{-1} along the major axis, and after correcting the inclination effect this is converted to $V_{\text{max}}(\text{corr}) = 145$ km s^{-1}. Based on our surface brightness profile, the galaxy is bulge dominated at $r = 6''$, at which radius $\sigma = 180$ km s^{-1} and $\epsilon = 0.1$ (taken from our ϵ-profile in Fig. 2). The obtained $V_{\text{max}}/\sigma = 0.8$, which at $\epsilon = 0.1$ means that the bulge is rotationally supported. In a similar manner V_{max}/σ values were found for the galaxies NGC 1553, NGC 3100, NGC 3706, and ESO 208-G21. For NGC 3100 we used $V_{\text{max}}(\text{corr}) = 120$ km s^{-1} and $\sigma = 190$ km s^{-1} (Carollo et al. 1993). The measurements were made at a position angle of $90°$, which deviates only $10°$ from the orientation of the major axis of the disk. In the bulge-dominated region at $r = 5''-10''$ this means that the bulge is rotationally supported. For NGC 1553 we use $V_{\text{max}}(\text{corr}) = 156$ km s^{-1} and $\sigma = 162$ km s^{-1} at $r = 10''$ (Kormendy 1984), which in this case also means that the bulge is rotationally supported. Quite interestingly, according to Kormendy the bright lens dominating at larger radial distances is hotter and not rotationally supported, indicating that *the lens is probably older than the bulge*. As expected, the elliptical galaxies NGC 3706 and ESO 208-G21 have neither kinematic nor photometric evidence of pseudobulges. Four of the galaxies in our sample have also either a nuclear ring, a secondary bar, or both, and generally the nuclear ring is currently forming stars. In conclusion, all galaxies with extended disks in our sample have some sign of a pseudobulge. Pseudobulges have been previously found in many late-type spiral galaxies (Carollo et al. 1998), and more recently in two early-type spiral galaxies (Kormendy et al. 2006) with Hubble types Sab and Sa.

Another interesting new finding of this study is that the bulges of two S0 galaxies in our sample are as small as in typical Sc-type spiral galaxies. For NGC 1411 $B/T = 0.08$, in comparison to 0.11 found in Sc galaxies. For NGC 3100 the bulge is also very small but could not be fitted in our decompositions. Both galaxies are dominated by lenses, NGC 1411 by a series of bright lenses and NGC 3100 by one dominant lens/oval. The bulge in NGC 1411 is disklike (has small n), but neither of the two galaxies has a nuclear

TABLE 8
MEAN PROPERTIES OF THE PRIMARY BARS FOR DIFFERENT HUBBLE TYPE BINS

Property	Sbc–Sm (OSU)	Sa-Sab (OSU+NOT+ESO)	S0/a (NOT+ESO)	S0 (NOT+ESO)
$\langle Q_g \rangle$..................................	0.26 ± 0.01	0.23 ± 0.02	0.18 ± 0.03	0.14 ± 0.02
$\langle A_2 \rangle$..................................	0.41 ± 0.02	0.66 ± 0.06	0.63 ± 0.06	0.49 ± 0.04
$\langle A_4 \rangle$..................................	0.17 ± 0.01	0.32 ± 0.04	0.29 ± 0.05	0.21 ± 0.03
$\langle r_{\mathrm{bar}}/h_r \rangle$.............................	0.91 ± 0.06	1.42 ± 0.11	1.72 ± 0.15	1.21 ± 0.13
$\langle r_{Qb}/h_r \rangle$.............................	0.57 ± 0.04	0.92 ± 0.07	1.07 ± 0.11	0.80 ± 0.08
N.......................................	57	19	10	10

NOTES.—OSU, the OSUBGS; NOT, the Nordic Optical Telescope. The errors are errors of the mean.

ring or other strong morphological signatures of strong star formation in the central regions of these galaxies. The bulge in NGC 1553 is most probably also extremely small, unless the inner disk (with obvious spiral arms) is considered a pseudobulge. To our knowledge NGC 1411 and NGC 3100 are the first candidates that might be analogs of Sc galaxies among S0 galaxies, having B/T flux ratios similar to those typically found in Sc galaxies. The existence of such galaxies has been suggested earlier in the DDO classification scheme by van den Bergh (1976, 1998). These two galaxies are extreme examples of S0 galaxies that would be difficult to explain by the merging of large disk galaxies. NGC 1411 is found to be a member of the Dorado group of 46 galaxies (Sandage 1975; Maia et al. 1989), which is one of the richest galaxy groups in the southern hemisphere. Using a more strict definition of a group, Garcia (1993) found the same galaxy to be a member of a small group of galaxies. NGC 1411 also has one major nearby companion, whereas NGC 3100 has many small nearby companions. Particularly in the case of NGC 1411, it is possible that a late-type spiral galaxy has transformed into an S0c type system through stripping mechanisms.

Ovals or lenses were found in 11 of the galaxies in our sample. Ovals have minor to major axis ratios between 0.85 and 0.89, in agreement with the previous estimations by Kormendy (1984) for typical ovals. However, the presence of lenses is more difficult to show, because their isophotes are not necessarily elongated. This is also the reason why they are not always detected while classifying galaxies. In the decompositions made in this study, the lenses can be best recognized using the model images (produced in the structural decompositions) that should have the observed galaxy morphologies. In many cases a good agreement between the model image and the observation was found only if a flat inner structure was also added to the fit. Galaxies with prominent lenses in our sample typically have multiple exponential parts in their surface brightness profiles.

Bars, bulges, and halos are related phenomena in galaxies. It has been shown by the theoretical models (see the review by Athanassoula 2005) that the properties of bars are formed in a complicated process between the halo and the disk, depending, for example, on the mass of the halo, the amount of halo mass in the resonances, or the mass distribution of the bulge. When these properties are favorable to angular momentum exchange between the halo and the disk, bars are expected to evolve over time, leading to more massive bars with larger quadrupole moments. As bars lose angular momentum in this process, these models also predict that bars gradually slow down. However, the models are still controversial. While the bar appears to slow down in most N-body models (Hernquist & Weinberg 1992; Debattista & Sellwood 2000; Athanassoula 2003; Sellwood 2003; Holley-Bockelmann et al. 2005), there are some other models in which the bar slow down is very small (Valenzuela & Klypin 2003). Also, because long bars in early-type disk galaxies are repeatedly found

to be fast-rotating systems (see the review by Debattista 2006), it is not clear that the longest bars are necessarily the most evolved bars. In this study it is interesting to look at whether the properties of bars in S0 galaxies are similar or fundamentally different from the properties of bars in early-type spiral galaxies.

In Table 8 we compare the mean properties of primary bars in different Hubble type bins. The properties for Sbc–Sm ($T = 4$–9) type galaxies are from Laurikainen et al. (2004b), based on a similar analysis for the galaxies in the OSUBGS. In order to increase the statistics for the Sa–Sab type spiral galaxies, the data are a collection from three samples: the OSUBGS, the sample of early-type disk galaxies in Paper I, and this study. There is a clear tendency showing that bar length increases from the late-type spiral galaxies toward the early-type spiral galaxies, as first suggested by Elmegreen & Elmegreen (1985). The maximum is reached for Hubble type S0/a, but bars in S0 galaxies are clearly shorter than bars in S0/a galaxies, although still longer than bars in late-type spiral galaxies. This is in agreement with the recent result obtained by Erwin (2005). The relative mass of the bar, as estimated from the A_2 and A_4 Fourier amplitudes of density, has a similar tendency. However, the bar-induced maximum tangential force, Q_g, decreases all the way from late-type spiral galaxies toward earlier types, reaching a minimum for S0 galaxies.

An interesting result in this study is that the properties of bars in the spiral-S0 divide, e.g., between the S0/a and S0 galaxies, are not exactly similar or explainable by the dilution effects of bulges. Bars in S0 galaxies are shorter (1.21 vs. 1.72) and less massive ($A_2 = 0.49$ vs. 0.63) than bars in S0/a galaxies. The fact that Q_g is slightly smaller in S0 galaxies is associated with the mass of the bar rather than the dilution by bulge, because the B/T ratios in S0 and S0/a galaxies are fairly similar ($Q_g = 0.24 \pm 0.14$ vs. 0.27 ± 0.17). The weaker bars in S0 galaxies might be due to a smaller amount of interstellar gas in these galaxies, which is expected to make the disks less reactive to bar formation. Bars in S0 galaxies might also be shorter and less massive because they are less evolved in time (see the models by Athanassoula 2003).

7. SUMMARY

A morphological analysis of a sample of 15 early-type disk galaxies, mainly S0 galaxies, has been presented in the K_s band. The sample is part of a more complete NIRS0S sample of 170 S0–S0/a galaxies, selected to have size and selection criteria similar to those for the OSUBGS sample for spiral galaxies. Our main idea is to characterize the properties of bars, ovals, and bulges for a large sample of galaxies in the spiral-S0 divide and to use this information to evaluate the origin of S0 galaxies and how they are related to spiral galaxies.

The galaxies were analyzed by applying Fourier methods for calculating the maximum gravitational torques and by applying a multicomponent 2D method for structural decompositions. A

generalized Sérsic function was used for the bulge and exponential function for the disk, whereas the other nonaxisymmetric components can be described either by a Sérsic or a Ferrers function. It was also possible to take into account the flattening and the shape parameter of the structures. For comparison, the 1D decomposition method was also used. We found that if only the bulge and the disk are fitted, 1D and 2D methods give fairly similar results ($\langle B/T \rangle = 0.55-0.48$).

Bars in the galaxies in our sample are typically surrounded by lenses, and four of the galaxies have double-bar/lens structures. Two of the galaxies classified as S0 galaxies in RC3 appeared to be elliptical galaxies (ESO 208-G21 and NGC 3706), and three of the nonbarred S0 galaxies were found to have inner disks (NGC 1411, NGC 3100, and NGC 1553). A previously nondetected nuclear ring was discovered in NGC 1387, and a nuclear bar was discovered in NGC 1326. We found that bars in S0 galaxies are not exactly similar to bars in S0/a galaxies: they are clearly shorter and less massive and have slightly weaker bar torques.

One of the most important results of this study is the finding that *11 nonelliptical galaxies in our sample show strong evidence of having disklike pseudobulges*; these bulges have surface brightness profiles that are closer to an exponential than to a de Vaucouleurs' type profile. Six of the galaxies also have either nuclear rings, nuclear bars, or nuclear disks. All galaxies in our sample have $B/T < 0.4$, as typically found in galaxies having pseudobulges. We find $\langle B/T \rangle = 0.25$ and $\langle n \rangle = 2$, thus confirming the earlier result in Paper I showing that bulges in S0 galaxies are considerably smaller and have more exponential surface brightness profiles than is assumed for their morphological types. A comparison to more simple 2D bulge-disk or 1D decompositions shows the importance of the multicomponent approach: these two methods give $\langle B/T \rangle = 0.55$ and 0.48, respectively, with the relative mass of the bulge being significantly overestimated in both cases. The value $\langle B/T \rangle = 0.55$ is close to the value 0.64 obtained by SGA04 for the early-type disk galaxies in the same wavelength using a 2D bulge-disk approach similar to that used in this study.

Quite interestingly, we also find two galaxies, NGC 1411 and NGC 3100, that due to their very small B/T flux ratios might be the proverbial analogs of Sc galaxies among classical S0 galaxies, as discussed in the DDO galaxy classification scheme by van den Bergh. These galaxies might be manifestations of galaxy evolution in the Hubble sequence, possibly formed by gas-stripping mechanisms from late-type spiral galaxies.

REFERENCES

Alonso-Herrero, A., Simpson, C., Ward, M., & Wilson, A. 1998, ApJ, 495, 196
Athanassoula, E. 2003, MNRAS, 341, 1179
———. 2005, Celest. Mech. Dyn. Astron., 91, 9
Athanassoula, E., Morin, S., Wozniak, H., Puy, D., Pierre, H., Lombard, J., & Bosma, A. 1990, MNRAS, 245, 130
Bekki, K., Warrick, J., & Yasuhiro, S. 2002, ApJ, 577, 651
Binney, J. 1980, MNRAS, 190, 421
Binney, J., & Merrifield, M. 1998, Galactic Astronomy (Princeton: Princeton Univ. Press)
Boisson, C., Joly, M., Pelat, D., & Ward, M. 2004, A&A, 428, 373
Buta, R. 1988, ApJS, 66, 233
———. 1990, ApJ, 351, 62
———. 1995, ApJS, 96, 39
Buta, R., Alpert, A., Cobb, M., Crocker, D., & Purcell, G. 1998, AJ, 116, 1142
Buta, R., & Block, D. 2001, ApJ, 550, 243
Buta, R., Byrd, G., & Freeman, T. 2004, AJ, 127, 1982
Buta, R., Corwin, H., & Odewahn, S. 2006a, The De Vaucouleurs Atlas of Galaxies (Cambridge: Cambridge Univ. Press) (BCO06)
Buta, R., & Crocker, D. 1991, AJ, 102, 1715
———. 1993, AJ, 105, 1344
Buta, R., Laurikainen, E., Salo, H., Block, D., & Knapen, J. 2006b, AJ, 132, 1852 (Paper II)
Buta, R., & Purcell, G. 1998, AJ, 115, 484
Buta, R., Treuthardt, P., Byrd, G., & Crocker, D. 2000, AJ, 120, 1289
Carollo, C., Danziger, I., & Buson, L. 1993, MNRAS, 265, 553
Carollo, C., Stiavelli, M., & Mack, J. 1998, AJ, 116, 68
Christlein, D., & Zabludoff, A. 2004, ApJ, 616, 192
Cid Fernandes, R., Jr., Storchi-Bergmann, T., & Schmitt, H. R. 1998, MNRAS, 297, 579
Combes, F., & Sanders, R. H. 1981, A&A, 96, 164
Corwin, H. G., de Vaucouleurs, A., & de Vaucouleurs, G. 1985, Southern Galaxy Catalogue (Austin: Univ. Texas)
Crocker, D., Baugus, P., & Buta, R. 1996, ApJS, 105, 353
Debattista, V. 2006, in ASP Conf. Ser. 352, New Horizons in Astronomy: Frank N. Bash Symposium, ed. S. J. Kannappan (San Francisco: ASP), 161
Debattista, V., & Sellwood, J. A. 2000, ApJ, 543, 704
de Grijs, R., Anders, P., Bastian, N., Lynds, R., Lamers, H., & O'Neil, E. 2003, MNRAS, 343, 1285
de Jong, R. 1996, A&A, 313, 45
de Souza, R., Gadotti, A., & dos Anjos, S. 2004, ApJS, 153, 411 (SGA04)

de Vaucouleurs, G. 1974, in IAU Symp. 58, Formation and Dynamics of Galaxies, ed. J. R. Shakeshaft (Dordrecht: Reidel), 1
de Vaucouleurs, G., & de Vaucouleurs, A. 1964, Reference Catalogue of Bright Galaxies (Austin: Univ. Texas)
de Vaucouleurs, G., de Vaucouleurs, A., Corwin, H., Buta, R. J., Paturel, G., & Fouqué, P. 1991, Third Reference Catalog of Bright Galaxies (New York: Springer)
Elmegreen, B. G., & Elmegreen, D. M. 1985, ApJ, 288, 438
Erwin, P. 2004, A&A, 415, 941
———. 2005, MNRAS, 364, 283
Eskridge, P., et al. 2002, ApJS, 143, 73
Evans, I., Koratkar, A., Storchi-Bergmann, T., Kirkpatrick, H., Heckman, T., & Wilson, A. 1996, ApJS, 105, 93
Ferruit, P., Wilson, A., & Mulchaey, J. 2000, ApJS, 128, 139
Friedli, D., Wozniak, H., Rieke, M., Martinet, L., & Bratschi, P. 1996, A&AS, 118, 461
Garcia, A. M. 1993, A&AS, 100, 47
Garcia-Barreto, J., Dettmar, R., Combes, F., Gerin, M., & Koribalski, B. 1991, Rev. Mex. AA, 22, 197
Garcia-Gomez, C., Barbera, C., Athanassoula, E., Bosma, A., & Whyte, L. 2004, A&A, 421, 595
Hawarden, T., van Woerden, H., Goss, W., Mebold, U., & Peterson, B. 1979, A&A, 76, 230
Hernquist, L., & Weinberg, M. 1992, ApJ, 400, 80
Holley-Bockelmann, K., Weinberg, M., & Katz, N. 2005, MNRAS, 363, 991
Jarvis, B., Dubath, P., Martinet, L., & Bacon, R. 1988, A&AS, 74, 513
Jungwiert, B., Combes, F., & Axon, D. 1997, A&AS, 125, 479
Kennicutt, R. C., Jr., et al. 2003, PASP, 115, 928
Kent, S. 1985, ApJS, 59, 115
Knapen, J. H., Mazzuca, L. M., Böker, T., Shlosman, I., Colina, L., Combes, F., & Axon, D. J. 2006, A&A, 448, 489
Kormendy, J. 1979, ApJ, 227, 714
———. 1984, ApJ, 286, 116
Kormendy, J., & Bender, R. 1996, ApJ, 464, L119
Kormendy, J., Cornell, M. E., Block, D., Knapen, J., & Allard, E. 2006, ApJ, 642, 765
Kormendy, J., & Kennicutt, R., Jr. 2004, ARA&A, 42, 603 (KK04)
Kuchinski, L., et al., 2000, ApJS, 131, 441
Laine, S., Shlosman, I., Knapen, J. H., & Peletier, R. F. 2002, ApJ, 567, 97
Lauer, T., et al. 2005, AJ, 129, 2138

Laurikainen, E., & Salo, H. 2000, A&AS, 141, 103
———. 2002, MNRAS, 337, 1118
Laurikainen, E., Salo, H., & Buta, R. 2004a, ApJ, 607, 103 (LSB04)
———. 2005, MNRAS, 362, 1319 (Paper I)
Laurikainen, E., Salo, H., Buta, R., & Vasylyev, S. 2004b, MNRAS, 355, 1251
Maia, M. A., da Costa, L. N., & Latham, D. W. 1989, ApJS, 69, 809
Maoz, D., Barth, A., Ho, L., Sternberg, A., & Filippenko, A. 2001, AJ, 121, 3048
Martel, A., et al. 2004, AJ, 128, 2758
Martini, P., Regan, M., Mulchaey, J., & Pogge, R. 2003, ApJS, 146, 353
Mulchaey, J., Regan, M., & Kundu, A. 1997, ApJS, 110, 299
Pahre, M. 1999, ApJS, 124, 127
Papovich, C., Giavalisco, M., Dickinson, M., Conselice, C., & Ferguson, H. 2003, ApJ, 598, 827
Peng, C., Ho, L., Impey, C., & Rix, H. 2002, AJ, 124, 266
Pfenniger, D. 1984, A&A, 134, 373
Phillips, A., Illingworth, G., MacKenty, J., & Franx, M. 1996, AJ, 111, 1566
Quillen, A., Frogel, J., & Gonzalez, R. 1994, ApJ, 437, 162
Raha, N., Sellwood, J., James, R., & Kahn, F. 1991, Nature, 352, 411
Rampazzo, R. 1988, A&A, 204, 81
Salo, H., Laurikainen, E., & Buta, R. 2004, in Penetrating Bars through Masks of Cosmic Dust, ed. D. Block et al. (Berlin: Springer), 673

Salo, H., Rautiainen, P., Buta, R., Purcell, G., Cobb, M., Crocker, D, & Laurikainen, E. 1999, AJ, 117, 792
Sandage, A. 1975, ApJ, 202, 563
Sandage, A., & Bedke, J. 1994, The Carnegie Atlas of Galaxies (Washington: Carnegie Inst.)
Sandage, A., & Brucato, R. 1979, AJ, 84, 472
Schwarz, M. 1981, ApJ, 247, 77
Schweizer, F. 1980, ApJ, 237, 303
Scorza, C., Bender, R., Winkelmann, C., Capaccioli, M., & Macchetto, D. F. 1998, A&AS, 131, 265
Sellwood, J. A. 2003, ApJ, 587, 638
Simkin, S., Su, H., & Schwarz, M. 1980, ApJ, 237, 404
Storchi-Bergmann, T., Rodriguez-Ardila, A., Schmitt, H., Wilson, A., & Baldwin, J. 1996, ApJ, 472, 83
Valenzuela, O., & Klypin, A. 2003, MNRAS, 345, 406
van den Bergh, S. 1976, ApJ, 206, 883
———. 1998, Galaxy Morphology and Classification (Cambridge: Cambridge Univ. Press)
Wozniak, H., Friedli, D., Martinet, P., & Bratschi, P. 1995, A&AS, 111, 115